Two-loop amplitude reduction with HELAC

Giuseppe Bevilacqua,[a] **Dhimiter Canko,**[b] **Costas Papadopoulos,**[a] **Aris Spourdalakis**[a,c,d]

[a] *Institute of Nuclear and Particle Physics, NCSR Demokritos, Patr. Grigoriou E' & 27 Neapoleos Str, 15341 Agia Paraskevi, Greece*

[b] *Dipartimento di Fisica e Astronomia, Università di Bologna e INFN, Sezione di Bologna, Via Irnerio 46, I-40126 Bologna, Italy*

[c] *University of Debrecen, Faculty of Science and Technology, Department of Experimental Physics, 4010, Debrecen, PO Box 105, Hungary*

[d] *Institute for Theoretical Physics, ELTE Eötvös Loránd University, Pázmány Péter sétány 1/A, H-1117 Budapest, Hungary*

Abstract: We present the computational framework HELAC2LOOP for the construction of the two-loop amplitude numerators and for their integrand-level reduction. CutTools-2 is the component of HELAC2LOOP that implements the numerical solution to the cut equations and the fitting of the coefficients of the basis [1]. Using recursive equations, we also show how to reconstruct numerically the numerators in $d = 4 - 2\epsilon$ dimensions, both at one- and two-loop levels. The analysis presented in this report, in conjunction with the ongoing development of the computational framework HELAC2LOOP, paves the road for the construction of an automated program for two-loop amplitude calculations for arbitrary scattering processes.

Keywords: Scattering Amplitudes, QCD Phenomenology, NNLO Computations

Contents

1 Introduction

Several decades after its establishment, the Standard Model (SM) keeps offering a successful description of Strong and Electroweak interactions among fundamental particles. One of the most concrete and reliable ways of probing the SM is the comparison of its predictions to experimental data from high-energy particle collisions. The present energy frontier is represented by the Large Hadron Collider (LHC) with its four experiments, CMS, ATLAS, ALICE, and LHCb. The forthcoming High Luminosity upgrade of the LHC (HL-LHC) will significantly boost the statistical accuracy of the experimental data that are being collected, allowing experiments to reach percent-level precision in many cases [2–4]. The accurate interpretation of the data from the LHC, as well as from possible future colliders [5], demands theoretical predictions of comparable precision.

Theoretical predictions are formulated from first principles within the framework of perturbative Quantum Field Theory, where scattering cross sections and other observables are computed as a power series expansion in the coupling constants of the SM. The first term in this expansion corresponds to the leading-order (LO) contribution, followed by subsequent corrections at next-to-leading order (NLO), next-to-next-to-leading order (NNLO), and so on. The calculation of NNLO corrections (and occasionally even $\mathrm{N^3LO}$) is necessary in order to meet the current (and near future) experimental precision. The bottleneck for most NNLO calculations consists, at present, of the computation of double-virtual corrections, which rely upon two-loop dimensionally regularized scattering amplitudes. As the number of particles in a process increases, the complexity of the latter increases dramatically. The current frontier is the calculation of $2 \to 3$ processes [6], with several results

in this direction being achieved in recent years [7–35] as the product of considerable effort from the theoretical community.

The calculation of two-loop amplitudes can be regarded as a three-step procedure. The initial step involves the construction of the amplitude through the use of standard Feynman graph generation [36, 37] or recursive approaches [38, 39]. The second step includes the reduction of the amplitude into a set of independent Feynman integrals, commonly known as *master integrals*. For this to be achieved, the constructed amplitude should be projected into a set of Feynman integrals, which can be done using tensor [40–44], or integrand [45–57] reduction methods. The generated Feynman integrals from these methods need to be furthermore reduced, at the integral level, into master integrals using *integration-by-parts* (IBP) identities [58–60], satisfied by the Feynman integrals within dimensional regularization ($d = 4 - 2\epsilon$). The latter field has benefited from the application of *finite-field techniques* [61, 62] for solving IBP identities, and the recent advancements in the generation of optimized IBP systems, utilizing *syzygy equations* [63, 64] and the *block-triangular form* [65, 66]. The last step for the computation of the scattering amplitude is the evaluation of the master integrals resulting from the reduction, which can be attained by methods such as *sector decomposition* [67–69], *differential equations* [70–75], *auxiliary mass flow* [76, 77], and *dimension-changing transformation* [78, 79].

The present report present the construction of the amplitude and the integrand-level reduction as implemented in the computational framework `HELAC2LOOP`. In the one-loop case, the integrand reduction *OPP method* [80], demonstrated a systematic algebraic approach to the computation of amplitudes, based upon solving *cut equations*, meaning equations resulting from setting some (or all) of the inverse propagators to zero, following a top-down approach. Integrand reduction has been implemented in various numerical algorithms [81–93] and has boosted automation of NLO computations. Our goal is to extend the OPP method to two-loop calculations [45–55]. Two-loop amplitude reduction at the integrand level in $d = 4 - 2\epsilon$ dimensions, following our recent publication [94], is implemented in the component of `HELAC2LOOP`, `CutTools-2`, by solving numerically cut equations and fitting the coefficients of the basis, generated by `BasisDet` [95]. In general, to facilitate computations, Feynman integrals that share the same topological and kinematical structure can be grouped into *integral families*. A novel element of our study is the extension of the cut equations to include all inverse propagators characterizing a provided integral family and not just the ones of the Feynman graph under consideration. This approach yields a larger number of systems of equations to be solved, albeit smaller in size, and has the advantage of allowing the reduction of all the Feynman graphs that belong to the same family altogether.

This report is structured as follows. In section 2, we review the construction of the two-loop amplitude numerators [39] and provide information for numerous processes with up to six particles. In section 3 we report on the details on the numerical implementation integrand-level reduction of the amplitude numerators as implemented in `CutTools-2`. In section 4, we present the new recursive equations that allow the numerical reconstruction of the amplitude numerators in $d = 4 - 2\epsilon$ dimensions, both at one- and two-loop levels, and their implementation in `HELAC1LOOP` and `HELAC2LOOP` respectively . In section 5, we conclude by giving a summary of our study and its prospects for the future.

2 Two-Loop HELAC algorithm

Before proceeding with the main discussion, we introduce the notation used throughout this work. A generic scattering process involving n external particles is specified by their flavours $\{f_1, f_2, \ldots, f_n\}$. Color degrees of freedom are treated in the *color-flow* representation [96], in which gluons (and their corresponding ghost and anti-ghost which can appear only within the loops) fields carry a pair of color indices $\{i, j\}$, while quarks and antiquarks are assigned $\{i, 0\}$ and $\{0, j\}$, respectively. Electroweak particles such as $W^{\pm}$, Z, γ, and the Higgs boson (denoted H) do not carry color and are therefore assigned the index pair $\{0, 0\}$. Within this representation, a color configuration is uniquely characterized by the product

$$C_F = \delta_{j_1}^{i_{\sigma_1}} \, \delta_{j_2}^{i_{\sigma_2}} \cdots \delta_{j_n}^{i_{\sigma_n}} \, , \tag{2.1}$$

where $\{\sigma_1, \sigma_2, \ldots, \sigma_n\}$ denotes a permutation of the set $\{1, 2, \ldots, n\}$. Consequently, for a process with n_g external gluons and n_q pairs of quarks, the number of independent color states is (see, e.g., Refs. [97, 98])

$$n_{cc} = (n_g + n_q)! \, . \tag{2.2}$$

The computation of tree-level scattering amplitudes within HELAC [98] is organised recursively. The fundamental objects in this construction are the so-called *currents*, i.e. tree-level sub-amplitudes associated with a subset $S_B \subset \{1, \ldots, n\}$ of the external particles. The currents are combined into sub-amplitudes of increasing complexity until the full amplitude is obtained. Each current is assigned a unique integer label

$$\mathrm{ID}(B) = \sum_{i \in S_B} 2^{\,i-1} \tag{2.3}$$

and a level, $Lvl(B)$, that counts the number of external particles that it consists.

Focusing now on the construction of two-loop integrands, the first step of the procedure involves the generation of *loop topologies*. All two-loop topologies describing arbitrary processes in the Standard Model[1] (SM) fall into one of the three master categories depicted in Fig. 1, which we refer to, for brevity, as "*Theta*", "*Infinity*", and "*Dumbbell*". The shaded regions K_i shown in these diagrams, which hereafter we will also refer to as *sectors*, represent schematically a collection of tree-level currents, $\{B_1, \ldots, B_{L_i}\}$, attached to the i-th propagator of the loop. To avoid confusion with currents that may include loop particles later on, these tree-level currents will from now on be referred to as *blobs*. Similarly, the labels A and B denote generic blobs that may be inserted at the loop vertices. The number of blobs appearing in each sector, together with their ordering, uniquely specifies a topology. We note, however, that this correspondence is not one-to-one: loop topologies are invariant under left-right and up-down reflections. In addition, *Theta* topologies exhibit a symmetry under arbitrary permutations of the sectors K_1, K_2, K_3. Configurations of blob orderings that are related by the aforementioned symmetries are identified and removed in order to

[1] More generally, this statement holds for any theory whose Feynman rules contain at most four-particle interaction vertices.

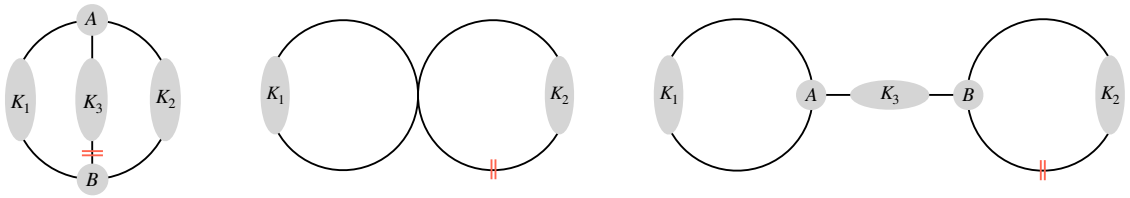

Figure 1: Master categories of two-loop topologies: *Theta* (a), *Infinity* (b), *Dumbbell* (c). The red lines indicate the propagator that is cut in order to express the two-loop topology as an equivalent $(n+2)$-particle process at one-loop.

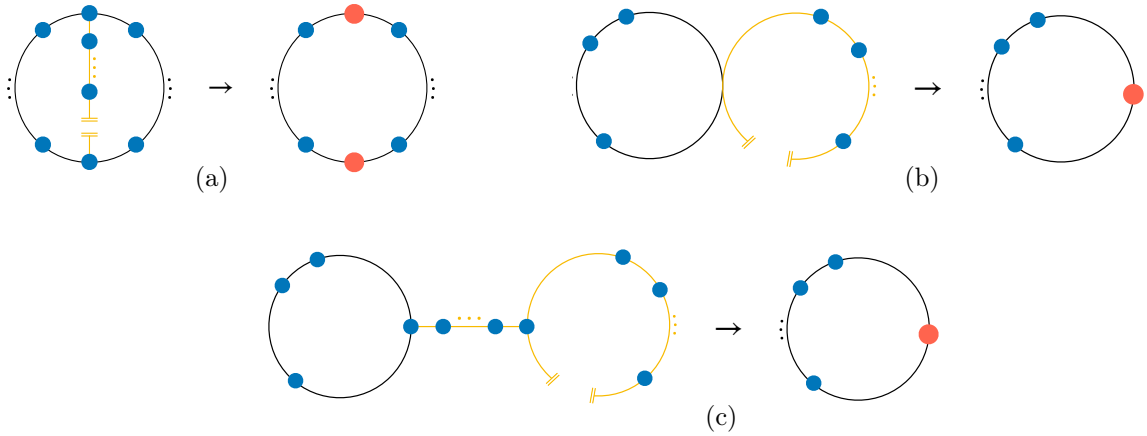

Figure 2: Relations between cut two-loop topologies and their corresponding one-loop configurations in $(n+2)$-particle kinematics: *Theta* (a), *Infinity* (b), and *Dumbbell* (c). The blobs represent tree-level currents attached to the loop propagators.

avoid double-counting. For the same reason, all *Theta* topologies are generated under the ordering

$$L_{K_1} \geq L_{K_2} \geq L_{K_3} \,, \tag{2.4}$$

where with L_{K_i} we denote the number of blobs that are attached in the sector K_i. Further details on the topological generation procedure can be found in Ref. [99].

The topologies generated at this stage do not yet contain any information regarding the flavor or color of the propagators in the loop. This information is introduced in the next step, referred to as *color-flavor dressing* (schematically illustrated in Fig. 3 for a simple example). The procedure can be summarised as follows:

1. We begin by cutting one propagator in the two-loop topology (using the conventions shown in Fig. 1). In this way, we obtain a one-loop topology describing an $(n+2)$-particle process with flavors

$$\{f_1, f_2, \ldots, f_n, F_{n+1}, F_{n+2}\} \,. \tag{2.5}$$

   We refer to this as the *equivalent one-loop configuration*. The flavors F_{n+1} and F_{n+2} correspond to the two additional particles generated by the cut, and may take any

value allowed to propagate in the loop. This step is illustrated in Fig. 2. In the diagrams, blobs are drawn using two distinct colours to emphasise that they are computed using different procedures. The blue blobs denote tree-level currents constructed via standard Dyson-Schwinger recursion, i.e. all sub-amplitudes compatible with the external-particle content are included. In contrast, the recursion defining the orange blobs is partially constrained by the non-trivial internal structure introduced by the presence of the cut loop propagator (shown in yellow).

2. Then we treat F_{n+1} and F_{n+2} as external particles with genuinely independent color degrees of freedom in the context of the one-loop process $\{f_1, f_2, \ldots, f_n, F_{n+1}, F_{n+2}\}$. This allows us to reuse, after suitable modifications, the framework for one-loop integrand construction already implemented in `HELAC-1LOOP` [85, 89]. Of course, the flavors and color indices of the cut-particles F_{n+1} and F_{n+2} are constrained by the requirement that they originate from cutting a specific propagator. As a consequence, our strategy introduces a redundant number of color degrees of freedom at this intermediate stage. These are eventually projected onto the lower-dimensional space describing the physical n-particle process using a contraction of the form

$$\left(\delta_{j_1}^{i_{\sigma_1}}\delta_{j_2}^{i_{\sigma_2}}\cdots\delta_{j_n}^{i_{\sigma_n}}\delta_{j_{n+1}}^{i_{\sigma_{n+1}}}\delta_{j_{n+2}}^{i_{\sigma_{n+2}}}\right)\left(\delta_{i_{n+2}}^{j_{n+1}}\delta_{i_{n+1}}^{j_{n+2}}\right) = (N_C)^{\alpha}\,\delta_{j_1}^{i_{\sigma'_1}}\delta_{j_2}^{i_{\sigma'_2}}\cdots\delta_{j_n}^{i_{\sigma'_n}}, \tag{2.6}$$

where $\{\sigma'_1, \ldots, \sigma'_n\}$ ($\{\sigma_1, \ldots, \sigma_{n+2}\}$) denotes a permutation of $\{1, \ldots, n\}$ ($\{1, \ldots, n+2\}$), N_C is the number of colors, and $\alpha = 0$ or 1 depending on the configuration.

3. Afterwards, using the one-loop configuration introduced in the previous step, the construction of the integrand proceeds according to the conceptual design of HELAC-1LOOP, but in an optimized form for improved efficiency. More specifically, the one-loop propagators are dressed with flavors in all ways compatible with the SM, and with colors by considering all configurations that preserve color flow at each loop vertex. The resulting one-loop topology is then cut once more, producing two additional external particles, F_{n+3} and F_{n+4}. This leads to a tree-level $(n+4)$-particle process with flavor content

$$\{f_1, f_2, \ldots, f_n, F_{n+1}, F_{n+2}, F_{n+3}, F_{n+4}\}\,. \tag{2.7}$$

At this stage, the computation of the one-loop numerator functions can be carried out using fully automated tree-level techniques [85, 89].

In the final step, a set of recursion relations is constructed for each two-loop topology per color connection and flavor structure of the loop particles (configuration). These relations encode the instructions required by `HELAC` for the numerical evaluation of the numerator of each configuration. They can be generated once and stored in a file referred to as the *skeleton*. For illustrative purposes, Fig. 4 shows an example of how a two-loop numerator is represented within our framework. The example corresponds to the 110th numerator out of a total of 332 numerators contributing to a specific color connection stored in the skeleton. Each line specifies the instructions for computing a single current appearing in

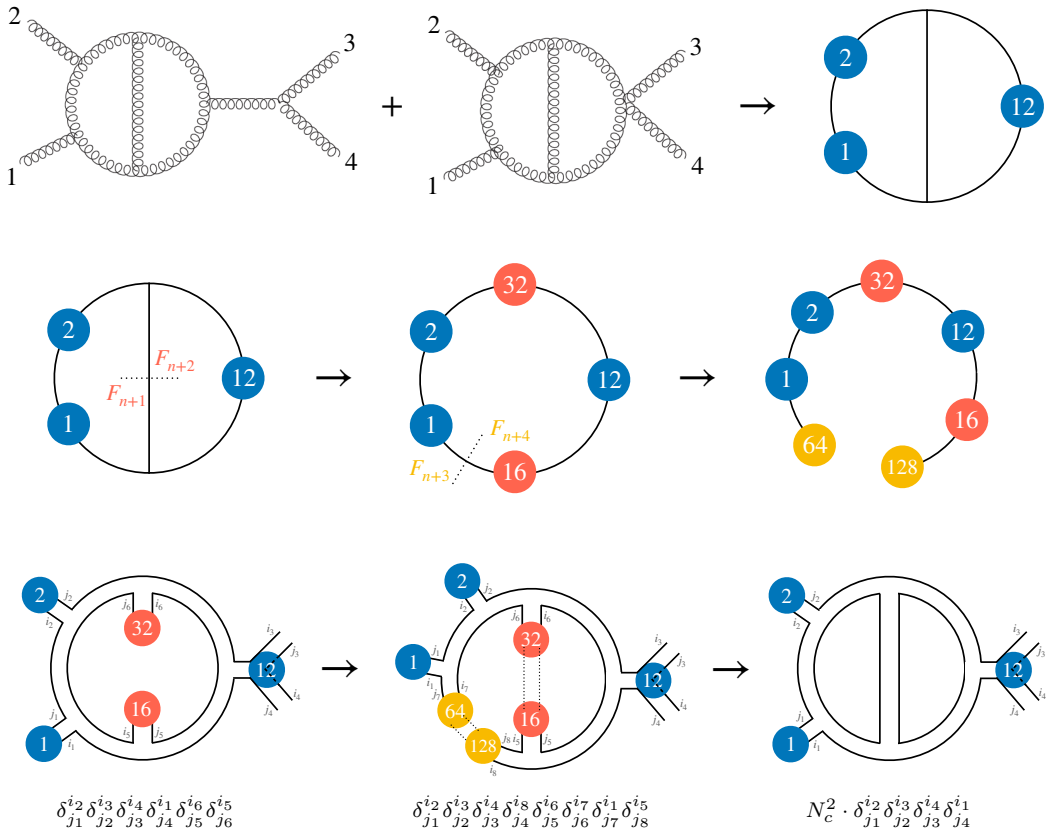

Figure 3: Schematic representation of the color and flavor dressing applied to a simple two-loop topology.

the recursive evaluation of the numerator. The information describing the underlying two-loop topology is contained in the final line. In particular, the first three entries encode the loop-propagator structure associated with the given numerator.

Aimed at the study of QCD corrections, the current implementation has been fully validated for processes involving only quarks (of all flavors), ghosts, and gluons circulating in the loops, and for up to six external particles. The external particles themselves may be any of the SM particles. Although not explicitly tested, the implementation should, after minor adjustments to the size of certain arrays, operate for an arbitrary number of external particles—disregarding, of course, potential efficiency and memory limitations of the machine used. To provide insight into the complexity and internal structure of the two-loop skeleton, we present in Appendix A detailed information on the skeleton associated with QCD corrections to SM processes at two loops, both in full color and in the leading-color approximation, as generated by `HELAC-2LOOP`.

We have performed a number of tests at the level of individual two-loop numerators in order to validate our implementation. Our results are in excellent agreement with the numerical output obtained using `FeynArts`+`FeynCalc` [36, 100].

```
 INFO NUM         110  of          332          7
 INFO ====================================
INFO   4  80  35   9   1   1  16  35   5  64  35   7   0   0   0   0   1   2
INFO   4  12  35  10   1   1   4  35   3   8  35   4   0   0   0   0   1   1
INFO   4  92  35  11   1   2  12  35  10  80  35   9   0   0   0   0   1   1
INFO   5  92  35  11   2   2   4  35   3   8  35   4  80  35   9   0   1   5
INFO   4 124  35  12   1   1  32  35   6  92  35  11   0   0   0   0   1   2
INFO   4 126  35  13   1   1   2  35   2 124  35  12   0   0   0   0   1   1
INFO   4 254  35  14   1   1 128  35   8 126  35  13   0   0   0   0   1   2
INFO   6   1  12   1   2  12  35  35  35  35  35  35   0   0   0   0   5   9
```

Figure 4: Representation of a two-loop numerator within the HELAC framework. All lines except the final one follow the same format as in HELAC-1LOOP [89]. The final line additionally contains information specific to the two-loop topology.

3 Numerical Reduction at two loops

In this section we present the basic elements of the numerical implementation of the algebraic reduction described in [1]. A generic unrenormalized L-loop scattering amplitude can be written schematically as

$$\mathcal{A}^{(L)}(\{p\}) = \sum_{g=1}^{G} \left(\int \prod_{i=1}^{L} [dk_i] \, \frac{\mathcal{N}(k_1, \ldots, k_L, \{p\})}{D_1 \, D_2 \, \cdots D_n} \right)_g , \tag{3.1}$$

where $k_1, \ldots, k_L$ are loop momenta, $[dk_i]$ denotes the integration measure associated to the loop momentum k_i, and $\{p\}$ represents the set of external kinematics. The amplitude consists generally of G partial contributions, individually denoted by g. Depending on the considered approach, the latter may be individual Feynman diagrams or consistently defined sub-amplitudes. In the following, we will refer to them as *loop topologies*. In what follows, we focus on the genuine two-loop contributions to the amplitude (so-called Theta topologies), namely those that cannot be trivially reduced to the product of one-loop ones (Infinity and Dumbbell topologies)[2]. Each loop topology is characterized by a *numerator* $\mathcal{N}$, which is a function of external momenta and wavefunctions as well as loop momenta, and by a product of n *inverse propagators* $D_1, \ldots, D_n$, appearing in its denominator[3].

Following reference [1] we seek to solve the following equation:

$$\mathcal{N} = P^{(N)} + \sum_{i=1}^{N} P_i^{(N-1)} D_i + \sum_{i=1}^{N-1} \sum_{j>i}^{N} P_{ij}^{(N-2)} D_i D_j + \ldots + P_{12\ldots N}^{(0)} D_1 D_2 \ldots D_N . \tag{3.2}$$

The first term in the right-hand of the above equation denotes the maximal cut, the second the next-to-maximal cut and so on. The parametrization of the polynomials P in terms of the so-called irreducible scalar products (ISP) [4] is obtained through the program `BasisDet` [47]. The latter provides a set of monomials, m_i $(i = 1, \ldots, M)$, which take the form $\prod_j \bar{z}_j^{r_j}$, where $\bar{z}_j$ denote ISP and r_j is an integer ranging from zero to some upper

[2] For the terminology, see Figure 1 of Ref. [101].

[3] Inverse propagators raised in higher integer powers must also be included to accommodate special contributions.

[4] For the definition of ISP see reference [1]

value calculated from the maximal tensor rank of the polynomial P with respect to k_1, k_2 and k_1, k_2 combined[5].

The algorithm to solve Eq. (3.2) can be described as follows. For each cut, all the relevant on-shell conditions are solved, determining the values of the 11 parameters, denoted by $\vec{X}$, i.e., the 4-dimensional components of k_1, k_2 and the μ_{ij} [6].Assuming that the set of monomials m_i $(i = 1, \ldots, M)$ parametrizing a given polynomial P is established,

$$P = \sum_{i=1}^{M} c_i m_i \tag{3.3}$$

then an $M \times M$ matrix, $\mathcal{M}$, is obtained by evaluating the monomials m_i on the solution to the cut equation, by assigning M random values to the free parameters of the vector $\vec{X}$, obtaining thus M instances of it, i.e. $\vec{X}_j$, $j = 1, \ldots, M$, and then computing the elements of the matrix $\mathcal{M}$, as follows:

$$\mathcal{M}_{i,j} \equiv m_i(\vec{X}_j). \tag{3.4}$$

The numerator $\mathcal{N}(\vec{X}, d)$ can be cast in the form

$$\mathcal{N} \equiv \mathcal{N}(\vec{X}, d) = \mathcal{N}_0 + \sum_{i \geq 1} \epsilon^i \mathcal{N}_\epsilon^{(i)}\,, \tag{3.5}$$

by expanding in powers of $\epsilon \equiv (4-d)/2$, where both $\mathcal{N}_0 \equiv \mathcal{N}(\vec{X}, d)|_{d=4}$ and $\mathcal{N}_\epsilon^{(i)} \equiv \mathcal{N}_\epsilon^{(i)}(\vec{X})$, are accessible numerically and depending on μ_{ij} through $\vec{X}$. These terms are used to calculate the $M \times 1$ matrices,

$$\mathcal{B}_j^{(0)} = \mathcal{N}_0(\vec{X}_j) \quad \mathcal{B}_j^{(i)} = \mathcal{N}_\epsilon^{(i)}(\vec{X}_j). \tag{3.6}$$

Then the given polynomial P is written explicitly as

$$P = \sum_{i=1}^{M} \left(c_i^{(0)} + \sum \epsilon^j \, c_i^{(j)} \right) m_i \tag{3.7}$$

where

$$\vec{c}^{\,(0)} = \mathcal{M}^{-1}\mathcal{B}^{(0)} \qquad \vec{c}^{\,(i)} = \mathcal{M}^{-1}\mathcal{B}^{(i)} \tag{3.8}$$

Once the polynomials of a given cut are determined they are subtracted from the original numerator. The resulting residual numerator is then subjected to the reduction procedure at the next cut, where one fewer propagator is placed on shell. The iterative process continues systematically, with each successive cut reducing the number of constraints, since one less propagator is on shell at each lower cut.

The above can be split into roughly two numerical solving algorithms, which we have implemented for a generic four external particle case:

- The numerical solution to the on-shell conditions for the propagators, i.e., the cut equations

[5] Corresponding to `RenormalizationCondition` in ref. [47].

[6] In $d = 4 - 2\epsilon$, $\mu_{ij} \equiv k_i^{(\epsilon)} \cdot k_j^{(\epsilon)}$, with $k^{(\epsilon)}$ the components of the loop momenta beyond $d = 4$ dimensions.

- The numerical solution of the matrix equations, Eq. 3.8, i.e., the polynomial fitting procedure.

Solving the cut-equations is performed by the iterative Levenberg–Marquardt method. This essentially amounts to a successive minimization of the least square distance and has the advantage of being completely generic in terms of the input of the external momenta. It works by starting from a random value for all parameters and iteratively minimizing the value of all propagators which are present in the relevant cut, up to an arbitrary tolerance. The fact that the cut equations do not determine all 11 parameters of $\vec{X}$ allows us to obtain an arbitrary number of different sets of solutions.

The numerical method used for solving the cut equations is the Levenberg-Marquardt algorithm [102], which iteratively solves the damped normal equations $(J^T J + \lambda I)\,\delta x = -J^T f$, where J is the Jacobian of the active equations, f is the residual vector, δx is the update step, and λ is a damping parameter controlling the interpolation between Gauss-Newton and gradient-descent behavior. The linear system is solved using Cholesky factorization, which decomposes the symmetric positive-definite matrix into an upper-triangular matrix and its transpose for efficient and stable solution of the normal equations. An Armijo backtracking line search [103] is used to adaptively scale the update step, ensuring that the residual decreases sufficiently at each iteration. Randomized restarts enhance robustness and help identify the solution with the smallest residual. The module `cutsols_all` solves systems of nine nonlinear equations in eleven variables corresponding to two four-momenta (k_1, k_2) and three auxiliary parameters $(\mu_{11}, \mu_{12}, \mu_{22})$. The equations are quadratic in the momenta, e.g., $(k_i + \sum_j p_j)^2 + \mu = 0$, where μ denotes collectively the ϵ-components of loop momenta, and the solver allows arbitrary subsets of equations to be masked, enabling treatment of under-constrained sets of cuts.

This is where the second step of the cut and fitting procedure comes in. The $M \times M$ matrix $\mathcal{M}$, Eq. 3.4, and the $M \times 1$ matrices, Eq. 3.6, are obtained by evaluating the monomials and the numerator on the solution to the cut equation, by assigning M random values to the free parameters of the vector $\vec{X}$. Then equations, Eq. 3.8, are solved using the linear solving `ZGESV LaPack` [104] algorithm. Note that we have compiled a quadruple precision version of `LaPack` in order to be able to solve the fitting and cut equations both in double and quadruple precision.

Finally, at each step of the iteration, an $N = N$ test [1] is performed, referring to the left- and right-hand sides of Eq. 3.2, to check the validity of the numerical algebraic reduction. This means that at each cut, the numerator minus the subtractions is calculated to confirm that the difference yields a numerical zero. This is done on values of the parameters on the relevant cut, other than those used in the fitting procedure, at each stage. At the final step of the recursion, the $N = N$ test is performed at completely random values of $\vec{X}$, thus ensuring that the reduction had been fully completed.

The code structure is as follows. A cut-fit routine is called in the main `HELAC2LOOP` framework. In turn, the cut-fit routine iteratively calls a routine which calculates the coefficients for the 9, 8, 7, 6, 5 and 4-cuts. Each of these subroutines has the following structure. For each individual cut, it calls the hard-coded monomial basis to determine the

number of cut solutions we need to calculate for the cut equations, since we need as many solutions as the number of monomials, Eq. 3.4. After obtaining the solutions and generating the system, a wrapper subroutine for `ZGESV` is called which returns the coefficients. After all the coefficients of each individual cut are calculated, the $N = N$ test is performed, checking that the fitting procedure has been properly completed for that cut, using solutions to the cut equations relevant to the cut in question. When the last cut (4-cut) is reached, the $N = N$ test is performed for the full numerator, on a completely random assignment of $\vec{X}$, thus verifying that the numerator is completely described by the final fitted polynomial.

The current version of the code works for four external particles. An extension for a higher number of external particles is under development. Moreover, the numerical precision of the fitting procedure at each step of the recursion is under investigation, so that we can improve the performance of the code.

4 Numerical reconstruction of numerators in $d = 4 - 2\varepsilon$

As described in Section 3, enabling HELAC to perform numerical computations of numerators in $d = 4-2\varepsilon$ dimensions is an important collateral task connected with the development of the reduction method. In this Section we describe the procedure that we have developed to accomplish this task.

Before starting the discussion, it is convenient to introduce some basic notation. Let us consider a generic scattering process described by n external particles, whose momenta are denoted $\{p\} \equiv \{p_1, \ldots, p_n\}$. Also, let q_1, q_2 be the two loop momenta. We work in the 't Hooft-Veltman regularisation scheme [105]. According to this scheme all external momenta are expressed in $d = 4$ dimensions, while $\bar{q}_1, \bar{q}_2$ as well as the Lorentz structures appearing in the loop vertices (either Dirac matrices or Lorentz metric tensors) live in $d = 4 - 2\varepsilon$ dimensions. Following Ref.[106], we adopt a bar to denote explicitly quantities living in d dimensions. We split the 4-dimensional and $(d-4)$-dimensional part of the latter quantities as follows,

$$\bar{q}_i^\alpha = q_i + \tilde{q}_i^\alpha \quad , \quad \bar{\gamma}^\alpha = \gamma^\alpha + \tilde{\gamma}^\alpha \quad , \quad \bar{g}^{\alpha\beta} = g^{\alpha\beta} + \tilde{g}^{\alpha\beta}. \tag{4.1}$$

The tilde quantities refer to genuine $(d-4)$-dimensional contributions, which satisfy the following relations:

$$\tilde{q}_i \cdot \tilde{q}_j = \mu_{ij} \quad , \quad \tilde{\gamma}^\alpha \tilde{\gamma}_\alpha = (d-4) \quad , \quad \tilde{g}^{\alpha\beta} \tilde{g}_{\alpha\beta} = (d-4). \tag{4.2}$$

The μ_{ij} can be identified with the quantities already introduced in Section 3. We remind that there is no intersection between the 4-dimensional and the $(d-4)$-dimensional subspaces, namely

$$\tilde{q}_i \cdot q_j = 0 \quad , \quad \tilde{\gamma}^\alpha \gamma_\alpha = 0 \quad , \quad \{\tilde{\gamma}^\alpha, \gamma^\beta\} = 0 \quad , \quad \tilde{g}^{\alpha\beta} g_{\alpha\beta} = 0. \tag{4.3}$$

By making repeated use of the rules of Eq. 4.1-4.3 in the computation of a generic two-loop numerator, one can cast the latter in the form:

$$\mathcal{N} = \sum_{i=0}^{i_{\max}} \varepsilon^i \, \mathcal{N}_i(\{p\}, q_1, q_2, \mu_{ij}). \tag{4.4}$$

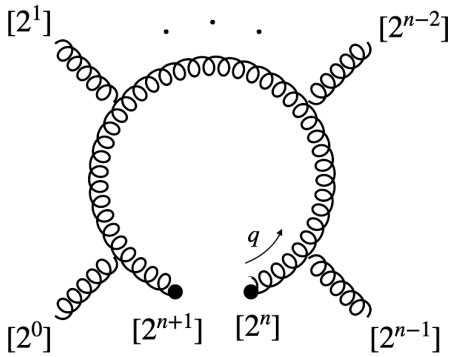

Figure 5: HELAC representation of a generic n-gluon one-loop topology. q denotes the loop momentum.

In words, Eq. 4.4 tells us that the numerator is made upon combination of a few building blocks, namely $p_i \cdot p_j$, $p_i \cdot q_j$ (purely four-dimensional quantities), μ_{ij} and $\varepsilon = (d-4)/2$. The genuine $(d-4)$-dimensional contribution consists of terms which depend on ε and/or μ_{ij}. We will also refer to the latter as *evanescent terms* in the following,

The method that we are developing aims at reconstructing the $(d-4)$-dimensional part of arbitrary one- and two-loop integrand numerators in QCD. In the first stage of development, we have focused on the pure Yang-Mills (YM) case (namely, only gluon and ghost interactions are taken into account). This allows us to perform first checks of our method in the context of n-gluon amplitude computations. Work is underway to extend the construction to include quark fields.

4.1 One-loop numerators

Let us consider a generic n-gluon amplitude at one loop, and let $\bar{q}$ be the loop momentum. According to standard HELAC representation, each external particle is labelled by an integer 2^i ($i = 0, 1, \ldots n-1$), see Figure 5. By opening one of the loop propagators, two extra external particles 2^n and 2^{n+1} are originated, carrying respectively momenta $\bar{q}$ and $-\bar{q}$ and polarisation vectors $\bar{\varepsilon}^\alpha_\lambda$ and $\bar{\omega}^\alpha_\lambda$ (λ denotes four possible states in which the latter appear). By construction, the polarisation vectors satisfy the completeness relation

$$\sum_\lambda \bar{\varepsilon}^\alpha_\lambda \, \bar{\omega}^\beta_\lambda = \bar{g}^{\alpha\beta} \, . \tag{4.5}$$

Figure 6 sketches how the recursive computation of numerators is organised in practice. At each stage of the recursion, a set of input currents is processed and an output current is computed. Schematically,

$$\bar{J}^{(n_1+n_2+\cdots+n_N)} = V_X(\bar{J}^{(n_1)}, \bar{J}^{(n_2)}, \cdots, \bar{J}^{(n_N)}) \, , \tag{4.6}$$

where V_X is the (color-flow decomposed) vertex function for the interaction vertex at hand. For example, for the three-gluon vertex we have

$$V^\alpha_{g_1 g_2 \to g}[\bar{J}^{(n_1)}, \bar{J}^{(n_2)}] \equiv \left(\bar{J}^{(n_2)} \cdot (2\,\bar{p}^{(n_1)} + \bar{p}^{(n_2)})\right) \bar{J}^{(n_1)\,\alpha}$$

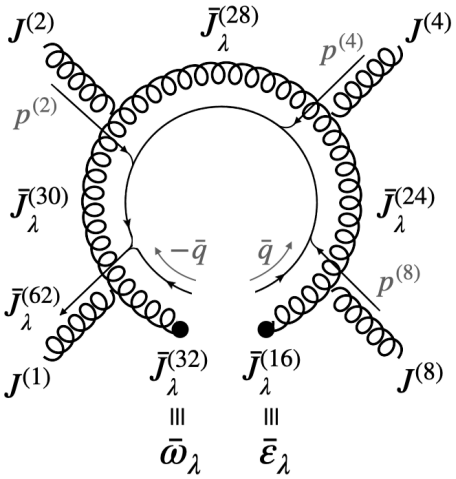

Figure 6: Sketch of recursive computation of the one-loop numerator for a representative $gg \to gg$ topology. The recursion starts from current $\bar{J}^{(16)}$ (particle 2^n) and flows towards $J^{(1)}$. Intermediate currents $\bar{J}^{(24)}_\lambda$, $\bar{J}^{(28)}_\lambda$, $\bar{J}^{(30)}_\lambda$, $\bar{J}^{(62)}_\lambda$ are computed along the recursion. Current $\bar{J}^{(16)}_\lambda$ marks the *loop start point*, while current $\bar{J}^{(32)}_\lambda$ marks the *loop end point*. The numerator is obtained as $\bar{N} = \sum_\lambda \left(\bar{J}^{(62)}_\lambda \cdot J^{(1)}_\lambda\right)$.

$$
\begin{aligned}
&- \left(\bar{J}^{(n_1)} \cdot (\bar{p}^{(n_1)} + 2\,\bar{p}^{(n_2)})\right) \bar{J}^{(n_2)\,\alpha} \\
&+ \left(\bar{J}^{(n_1)} \cdot \bar{J}^{(n_2)}\right) \left(\bar{p}^{(n_2)} - \bar{p}^{(n_1)}\right)^\alpha
\end{aligned}
\tag{4.7}
$$

where $\bar{p}^{(n_1)}, \bar{p}^{(n_2)}$ are the momenta associated with the two input currents (assumed incoming). The full list of vertex functions relevant for the case of pure YM QCD are reported in Appendix B. The recursion starts from the loop vertex which involves particle 2^n and flows towards particle $2^0 = 1$ (see also References [85, 98] for more details). In the shown example, current $\bar{J}^{(62)}_\lambda$ marks the endpoint of the recursion. The full numerator is obtained as

$$
\bar{N}(\{p\}, \bar{q}) = \sum_\lambda \left(\bar{J}^{(62)}_\lambda \cdot J^{(1)}\right) . \tag{4.8}
$$

We note that current $J^{(1)}$ is unbarred, since in the 't Hooft-Veltman scheme all wavefunctions and momenta of physical external particles live in $d = 4$ dimensions. Conversely, all currents whose momentum explicitly depends on $\bar{q}$ acquire a $(d-4)$-dimensional part. The problem that we are addressing can be formulated as follows: find a method to reconstruct the $(d-4)$-dimensional part of a recursive current (computed either analytically or numerically) knowing its $d = 4$ component. Schematically:

$$
J^{(N)} \to \bar{J}^{(N)} = J^{(N)} + \mathcal{E}\left[\, J^{(N)} \,\right], \tag{4.9}
$$

where $\mathcal{E}[\cdot]$ is a formal operator which generates all ε and $\mu \equiv \tilde{q}^2$ terms associated with an input $d = 4$ quantity.

Reconstructing the evanescent terms in the context of an *analytic* calculation is a trivial task which can be accomplished by use of the rules:

$$\begin{aligned}
&\mathcal{E}\,[\,q^2\,X\,] = \mu\,X\,,\\
&\mathcal{E}\,[\,\sum_\lambda (\varepsilon_\lambda\cdot\omega_\lambda)\,X\,] = (d-4)\,X\,,\\
&\mathcal{E}\,[\,\sum_\lambda (\varepsilon_\lambda\cdot q)\,(\omega_\lambda\cdot q)\;X\,] = \mu\,X\,.
\end{aligned} \tag{4.10}$$

This is possible on condition that the structure of the individual terms entering the expression of a current are known, which is clearly not the case when fully *numeric*, recursive computations are performed. Crucially, there are only few critical Lorentz structures which, upon combination, can generate evanescent terms at any step of the recursion. For the pure YM case they are the following ones: $\{\,\tilde{q}^\alpha,\,\tilde{\varepsilon}^\alpha,\,(\tilde{\varepsilon}\cdot\tilde{q}),\,(\tilde{\varepsilon}\cdot\tilde{q})\,\tilde{q}^\alpha,\,\mu,\,(d-4)\}$[7]. Thus, we are allowed to express the most general $(d-4)$-dimensional structure of a vector current $J^{(N)\,\alpha}$, at one loop, in the following way:

$$\begin{aligned}
\mathcal{E}\,[\,J^{(N)\,\alpha}\,] \;\equiv\; & C_q^{(N)}\,\tilde{q}^\alpha \;+\; C_\varepsilon^{(N)}\,\tilde{\varepsilon}^\alpha \;+\; J_{\varepsilon q}^{(N)\,\alpha}\,(\tilde{\varepsilon}\cdot\tilde{q}) \;+\; C_{\varepsilon q,q}^{(N)}\,(\tilde{\varepsilon}\cdot\tilde{q})\,\tilde{q}^\alpha\\
& +\; J_\mu^{(N)\,\alpha} \;+\; (d-4)\,J_{d-4}^{(N)\,\alpha}\,.
\end{aligned} \tag{4.11}$$

Each critical structure comes along with a coefficient (either scalar or vector) which is a function of pure $d=4$ quantities. Like the currents themselves, these coefficients satisfy a set of recursion relations which vary upon the vertex. Recursive equations are derived by plugging Eq. 4.11 into Eq. 4.6. To each input current $J^{(n_i)}$ we associate an integer $L^{(n_i)}$, defined as follows:

$$\begin{aligned}
&L^{(n_i)} = 0 \quad \text{if the current does not belong to a loop propagator}\,;\\
&L^{(n_i)} = 1 \quad \text{if the current belongs to a loop propagator}\,;\\
&L^{(n_i)} = 2 \quad \text{if } n_i = 2^{n+1} \text{ (loop endpoint)}\;\;.
\end{aligned} \tag{4.12}$$

We will refer to the latter integer with the name of *loop number*.

The structured of recursive equations for the one-loop case is rather compact and is reported below. For the case of $g_1g_2\to g$ vertex, they read:

$$\begin{aligned}
C_q^{(n_1+n_2)} = {} & \theta(L^{(n_1)})\;C_q^{(n_1)}\,J^{(n_2)}\cdot\Big(2\,p^{(n_1)}+p^{(n_2)}\Big) - \theta(L^{(n_2)})\;C_q^{(n_2)}\,J^{(n_1)}\cdot\Big(p^{(n_1)}+2\,p^{(n_2)}\Big)\\
& + \Big(\theta(L^{(n_2)})-\theta(L^{(n_1)})\Big)\;J^{(n_1)}\cdot J^{(n_2)}
\end{aligned} \tag{4.13}$$

$$\begin{aligned}
C_\varepsilon^{(n_1+n_2)} = {} & \theta(L^{(n_1)})\;C_\varepsilon^{(n_1)}\,J^{(n_2)}\cdot\Big(2\,p^{(n_1)}+p^{(n_2)}\Big)\\
& - \theta(L^{(n_2)})\;C_\varepsilon^{(n_2)}\,J^{(n_1)}\cdot\Big(p^{(n_1)}+2\,p^{(n_2)}\Big)
\end{aligned} \tag{4.14}$$

$$\begin{aligned}
J_{\varepsilon q}^{(n_1+n_2)\,\alpha} = {} & \theta(L^{(n_1)})\;\Big(V^\alpha_{g_1g_2\to g}\,[\bar{J}_{\varepsilon q}^{(n_1)},\bar{J}^{(n_2)}] \;-\; J^{(n_1)\,\alpha}\Big(C_\varepsilon^{(n_1)}+\mu\,C_{\varepsilon q,q}^{(n_1)}\Big)\Big)\\
& + \theta(L^{(n_2)})\;\Big(V^\alpha_{g_1g_2\to g}\,[\bar{J}^{(n_1)},\bar{J}_{\varepsilon q}^{(n_2)}] \;+\; J^{(n_2)\,\alpha}\Big(C_\varepsilon^{(n_2)}+\mu\,C_{\varepsilon q,q}^{(n_2)}\Big)\Big)
\end{aligned} \tag{4.15}$$

[7] from now on we will drop the index λ to make notation lighter

$$C_{\varepsilon q,q}^{(n_1+n_2)} = \theta(L^{(n_1)})\,\left(J_{\varepsilon q}^{(n_1)}\cdot J^{(n_2)} + C_{\varepsilon q,q}^{(n_1)}\,J^{(n_2)}\cdot\left(2\,p^{(n_1)}+p^{(n_2)}\right)\right)$$
$$+\,\theta(L^{(n_2)})\,\left(J^{(n_1)}\cdot J_{\varepsilon q}^{(n_2)} - C_{\varepsilon q,q}^{(n_2)}\,J^{(n_1)}\cdot\left(p^{(n_1)}+2\,p^{(n_2)}\right)\right) \tag{4.16}$$

$$J_{\mu}^{(n_1+n_2)\,\alpha} = \theta(L^{(n_1)})\left(-\mu\,C_q^{(n_1)}\,J^{(n_2)\,\alpha}\right) + \theta(L^{(n_2)})\left(\mu\,C_q^{(n_2)}\,J^{(n_1)\,\alpha}\right)$$
$$+\,\theta(L^{(n_1)})\,\theta(L^{(n_2)}-1)\left(2\,\mu\,C_q^{(n_1)}\,J^{(n_2)\,\alpha} + \mu\,J_{\varepsilon q}^{(n1)\,\alpha} + \mu\,C_{\varepsilon q,q}^{(n1)}\,\left(p^{(n_2)}-p^{(n_1)}\right)^{\alpha}\right)$$
$$+\,\theta(L^{(n_1)}-1)\,\theta(L^{(n_2)})\left(-2\,\mu\,C_q^{(n_2)}\,J^{(n_1)\,\alpha} - \mu\,J_{\varepsilon q}^{(n2)\,\alpha} + \mu\,C_{\varepsilon q,q}^{(n_2)}\,\left(p^{(n_2)}-p^{(n_1)}\right)^{\alpha}\right) \tag{4.17}$$

$$J_{(d-4)}^{(n_1+n_2)\,\alpha} = \theta(L^{(n_1)})\,\theta(L^{(n_2)}-1)\left(C_{\varepsilon}^{(n_1)}\,\left(p^{(n_2)}-p^{(n_1)}\right)^{\alpha}\right)$$
$$+\,\theta(L^{(n_1)}-1)\,\theta(L^{(n_2)})\left(C_{\varepsilon}^{(n_2)}\,\left(p^{(n_2)}-p^{(n_1)}\right)^{\alpha}\right) \tag{4.18}$$

The initial condition for the recursive equations above is set at the loop start point[8]:

$$C_q^{(2^{n-1})} = J_{\varepsilon q}^{(2^{n-1})\,\alpha} = C_{\varepsilon q,q}^{(2^{n-1})} = 0 \quad ; \quad C_{\varepsilon}^{(2^{n-1})} = 1 \tag{4.19}$$

Similarly, the recursion relations for the $g_1g_2g_3 \to g$ vertex read:

$$C_q^{(n_1+n_2+n_3)} = \theta(L^{(n_1)})\,\left(2\,C_q^{(n_1)}\,J^{(n_2)}\cdot J^{(n_3)}\right) + \theta(L^{(n_2)})\,\left(-C_q^{(n_2)}\,J^{(n_1)}\cdot J^{(n_3)}\right)$$
$$+\,\theta(L^{(n_3)})\,\left(-C_q^{(n_3)}\,J^{(n_1)}\cdot J^{(n_2)}\right) \tag{4.20}$$

$$C_{\varepsilon}^{(n_1+n_2+n_3)} = \theta(L^{(n_1)})\,\left(2\,C_{\varepsilon}^{(n_1)}\,J^{(n_2)}\cdot J^{(n_3)}\right) + \theta(L^{(n_2)})\,\left(-C_{\varepsilon}^{(n_2)}\,J^{(n_1)}\cdot J^{(n_3)}\right)$$
$$+\,\theta(L^{(n_3)})\,\left(-C_{\varepsilon}^{(n_3)}\,J^{(n_1)}\cdot J^{(n_2)}\right) \tag{4.21}$$

$$J_{\varepsilon q}^{(n_1+n_2+n_3)\,\alpha} = \theta(L^{(n_1)})\,\left(V_{g_1g_2g_3\to g}^{\alpha}[\bar{J}_{\varepsilon q}^{(n_1)},\bar{J}^{(n_2)},\bar{J}^{(n_3)}]\right)$$
$$+\,\theta(L^{(n_2)})\,\left(V_{g_1g_2g_3\to g}^{\alpha}[\bar{J}^{(n_1)},\bar{J}_{\varepsilon q}^{(n_2)},\bar{J}^{(n_3)}]\right)$$
$$+\,\theta(L^{(n_3)})\,\left(V_{g_1g_2g_3\to g}^{\alpha}[\bar{J}^{(n_1)},\bar{J}^{(n_2)},\bar{J}_{\varepsilon q}^{(n_3)}]\right) \tag{4.22}$$

$$C_{\varepsilon q,q}^{(n_1+n_2+n_3)} = \theta(L^{(n_1)})\,\left(2\,C_{\varepsilon q,q}^{(n_1)}\,J^{(n_2)}\cdot J^{(n_3)}\right) + \theta(L^{(n_2)})\,\left(-C_{\varepsilon q,q}^{(n_2)}\,J^{(n_1)}\cdot J^{(n_3)}\right)$$
$$+\,\theta(L^{(n_3)})\,\left(-C_{\varepsilon q,q}^{(n_3)}\,J^{(n_1)}\cdot J^{(n_2)}\right) \tag{4.23}$$

$$J_{\mu}^{(n_1+n_2+n_3)\,\alpha} = \theta(L^{(n_1)})\,\theta(L^{(n_2)}-1)\left(-\mu\,C_{\varepsilon q,q}^{(n_1)}\,J^{(n_3)\,\alpha}\right)$$
$$+\,\theta(L^{(n_1)})\,\theta(L^{(n_3)}-1)\left(-\mu\,C_{\varepsilon q,q}^{(n_1)}\,J^{(n_2)\,\alpha}\right)$$
$$+\,\theta(L^{(n_2)})\,\theta(L^{(n_1)}-1)\left(-\mu\,C_{\varepsilon q,q}^{(n_2)}\,J^{(n_3)\,\alpha}\right)$$
$$+\,\theta(L^{(n_2)})\,\theta(L^{(n_3)}-1)\left(2\,\mu\,C_{\varepsilon q,q}^{(n_2)}\,J^{(n_1)\,\alpha}\right)$$
$$+\,\theta(L^{(n_3)})\,\theta(L^{(n_1)}-1)\left(-\mu\,C_{\varepsilon q,q}^{(n_3)}\,J^{(n_2)\,\alpha}\right)$$
$$+\,\theta(L^{(n_3)})\,\theta(L^{(n_2)}-1)\left(2\,\mu\,C_{\varepsilon q,q}^{(n_3)}\,J^{(n_1)\,\alpha}\right) \tag{4.24}$$

[8]Currents which are not associated to a loop propagator have zero coefficients, since they are pure $d=4$ quantities in t'Hooft-Veltman scheme

$$
\begin{aligned}
J^{(n_1+n_2+n_3)\,\alpha}_{(d-4)} &= \theta(L^{(n_1)})\,\theta(L^{(n_2)}-1)\left(-C^{(n_1)}_{\tilde{\varepsilon}}\,J^{(n_3)\,\alpha}\right)\\
&+\theta(L^{(n_1)})\,\theta(L^{(n_3)}-1)\left(-C^{(n_1)}_{\tilde{\varepsilon}}\,J^{(n_2)\,\alpha}\right)\\
&+\theta(L^{(n_2)})\,\theta(L^{(n_1)}-1)\left(-C^{(n_2)}_{\tilde{\varepsilon}}\,J^{(n_3)\,\alpha}\right)\\
&+\theta(L^{(n_2)})\,\theta(L^{(n_3)}-1)\left(2\,C^{(n_2)}_{\tilde{\varepsilon}}\,J^{(n_1)\,\alpha}\right)\\
&+\theta(L^{(n_3)})\,\theta(L^{(n_1)}-1)\left(-C^{(n_3)}_{\tilde{\varepsilon}}\,J^{(n_1)\,\alpha}\right)\\
&+\theta(L^{(n_3)})\,\theta(L^{(n_2)}-1)\left(2\,C^{(n_3)}_{\tilde{\varepsilon}}\,J^{(n_2)\,\alpha}\right)
\end{aligned}
\tag{4.25}
$$

We are left to deal with ghost-gluon interactions. Given the scalar nature of a ghost current, the general form of its $(d-4)$ structure looks simpler:

$$
\mathcal{E}\,[\,J^{(N)}_{\rm ghost}\,] \equiv C^{(N)}_{\tilde{\varepsilon}q}\,(\tilde{\varepsilon}\cdot\tilde{q}) \,+\, J^{(N)}_{\mu} \,+\, (d-4)\,J^{(N)}_{d-4} \tag{4.26}
$$

In fact, it is easy to show that $\mathcal{E}\,[\,J^{(N)}_{\rm ghost}\,]=0$ at one loop. Indeed ghost topologies appear always in the form of closed-ghost loops. Given that no gluon propagator appears in the loop, there is no way to generate $(\tilde{\varepsilon}\cdot\tilde{q})$ terms along the recursion, hence $C^{(N)}_{\tilde{\varepsilon}q}=0$. For the same reason, neither μ nor $(d-4)$ terms can be generated at any step of the recursive computation.

The recursive equations described so far, have been implemented in a new version `HELAC1LOOP_DDIM`. We have validated the numerical implementation of the recursive equations at one loop against analytic results from FeynCalc [100]. Moreover, we have tested that the results obtained from the new version, regarding $gg\to gg$ and $gg\to ggg$ one-loop amplitudes, are in complete agreement with those provided by the existing `HELAC-1LOOP` [89] code [9].

4.2 Two-loop numerators

In order to address two-loop numerators we use a generalization of the ideas elaborated in Section 4.1. Now we have two loop momenta $(\bar{q}_1,\bar{q}_2)$ and four extra particles $(2^n,\ldots 2^{n+3})$ originated after opening two of the loop propagators (see Figure 7). The polarization vectors associated to the latter particles are respectively $\bar{\varepsilon}_2,\bar{\omega}_2,\bar{\varepsilon}_1,\bar{\omega}_1$.

In what follows, we focus on the genuine two-loop contributions to the amplitude (so-called *Theta* topologies), namely those that cannot be trivially reduced to the product of one-loop ones (*Infinity* and *Dumbbell* topologies).

The origin of evanescent terms for the two-loop case can be tracked down to the following relations:

$$
\begin{aligned}
&\mathcal{E}\,[\,(q_i\cdot q_j)\,X\,] = \mu_{ij}\,X\,,\\
&\mathcal{E}\,[\,\sum_{\lambda}(q_i\cdot\varepsilon_{k,\lambda})\,(q_j\cdot\omega_{k,\lambda})\,X\,] \;=\; \mu_{ij}\,X\,,\\
&\mathcal{E}\,[\,\sum_{\lambda}(\varepsilon_{i,\lambda}\cdot\omega_{i,\lambda})\;X\,] \;=\; (d-4)\,X\,,
\end{aligned}
$$

[9] A file named `benchmark_comparisons_4g_5g_pureYM.txt` is attached to this report.

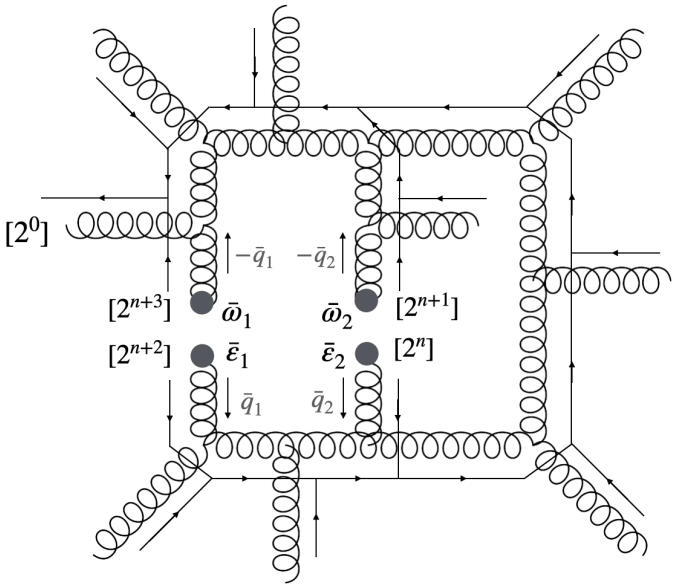

Figure 7: HELAC representation of a generic n-gluon two-loop numerator and flow of recursive computation. Current 2^{n+2} marks the loop start point, 2^{n+3} the loop end point.

$$
\begin{aligned}
\mathcal{E}\,[\,\sum_{\lambda_1,\lambda_2}(\varepsilon_{1,\lambda_1}\cdot\omega_{1,\lambda_1})\,(\varepsilon_{2,\lambda_2}\cdot\omega_{2,\lambda_2})\;X\,] \;&=\; (d-4)\,X\,,\\
\mathcal{E}\,[\,\sum_{\lambda_1,\lambda_2}(\varepsilon_{1,\lambda_1}\cdot\omega_{2,\lambda_2})\,(\varepsilon_{2,\lambda_2}\cdot\omega_{1,\lambda_1})\;X\,] \;&=\; (d-4)\,X\,,\\
\mathcal{E}\,[\,\sum_{\lambda_1,\lambda_2}(\varepsilon_{1,\lambda_1}\cdot\varepsilon_{2,\lambda_2})\,(\omega_{1,\lambda_1}\cdot\omega_{2,\lambda_2})\;X\,] \;&=\; (d-4)\,X
\end{aligned}
\tag{4.27}
$$

Moving along the same path set in Section 4.1, it is possible to list down all the critical Lorentz structures leading to evanescent terms during the recursion. For two-loop numerator computations, the most general $(d-4)$-dimensional structure of a vector current reads:

$$
\begin{aligned}
\mathcal{E}\,[\,J^{(N)\,\alpha}\,] \;\equiv\; &\sum_{i=1}^{2} C^{(N)}_{q_i}\,\tilde{q}_i^{\,\alpha} \;+\; \sum_{i=1}^{2} C^{(N)}_{\varepsilon_i}\,\tilde{\varepsilon}_i^{\,\alpha} \;+\; C^{(N)}_{\omega_2}\,\tilde{\omega}_2^{\,\alpha}\\
&+\; \sum_{i,j=1}^{2} J^{(N)\,\alpha}_{\varepsilon_i q_j}\,(\tilde{\varepsilon}_i\cdot\tilde{q}_j) \;+\; J^{(N)\,\alpha}_{\omega_2 q_2}\,(\tilde{\omega}_2\cdot\tilde{q}_2)\\
&+\; J^{(N)\,\alpha}_{\varepsilon_1\varepsilon_2}\,(\tilde{\varepsilon}_1\cdot\tilde{\varepsilon}_2) \;+\; \sum_{i,j=1}^{2} J^{(N)\,\alpha}_{\varepsilon_1 q_i \varepsilon_2 q_j}\,(\tilde{\varepsilon}_1\cdot\tilde{q}_i)(\tilde{\varepsilon}_2\cdot\tilde{q}_j)\\
&+\; \sum_{i,j,k=1}^{2} C^{(N)}_{\varepsilon_i q_j, q_k}(\tilde{\varepsilon}_i\cdot\tilde{q}_j)\,\tilde{q}_k^{\,\alpha} \;+\; \sum_{i,j,k\neq i}^{2} C^{(N)}_{\varepsilon_i q_j, \varepsilon_k}(\tilde{\varepsilon}_i\cdot\tilde{q}_j)\,\tilde{\varepsilon}_k^{\,\alpha}\\
&+\; C^{(N)}_{\omega_2 q_2, q_2}(\tilde{\omega}_2\cdot\tilde{q}_2)\,\tilde{q}_2^{\,\alpha} \;+\; \sum_{i=1}^{2} C^{(N)}_{\varepsilon_1\varepsilon_2, q_i}(\tilde{\varepsilon}_1\cdot\tilde{\varepsilon}_2)\,\tilde{q}_i^{\,\alpha}
\end{aligned}
$$

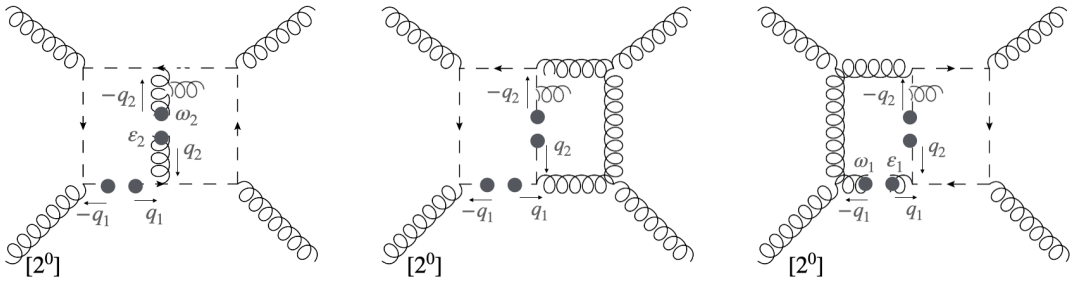

Figure 8: Representative two-loop examples of topologies containing ghosts.

$$+ \sum_{i,j,k=1}^{2} C^{(N)}_{\varepsilon_i q_j, \varepsilon_k} (\tilde{\varepsilon}_1 \cdot \tilde{q}_i)(\tilde{\varepsilon}_2 \cdot \tilde{q}_j) \tilde{q}_k^{\alpha}$$
$$+ J^{(N)\,\alpha}_{\mu} + \sum_{m} (d-4)^m J^{(N)\,\alpha}_{(d-4),m} \tag{4.28}$$

where $J^{(N)\,\alpha}_{\mu}$ contains all μ_{ij}-dependent terms at $\mathcal{O}((d-4)^0)$, while $J^{(N)\,\alpha}_{(d-4),m}$ denotes $\mathcal{O}((d-4)^m)$ contributions. Let us note that also the latter contributions may contain μ_{ij}-dependent terms. Concerning ghost currents, we can write most generally:

$$\mathcal{E}\,[\,J^{(N)}_{\rm ghost}\,] \equiv \sum_{i=1}^{2} C^{(N)}_{\varepsilon_i q_i}\,(\tilde{\varepsilon}_i \cdot \tilde{q}_i) \;+\; J^{(N)}_{\mu} \tag{4.29}$$

Let us note that, at two loops, ghost topologies can accommodate gluon propagators in the loop. Figure 8 shows representative examples for the process $gg \to ggg$. This implies that the coefficient $C^{(N)}_{\varepsilon_i q_i}$ in Eq. 4.29 can be non-zero, and μ_{ij} terms can be generated along the recursion. Still no $\mathcal{O}((d-4))$ terms can be generated at any stage of the recursion.

The decomposition of Eq. 4.28 can be applied to derive fully general recursive equations for three-gluon and four-gluon vertices. We note, however, that only a subset of those coefficients is involved at each step of the recursion. For an arbitrary *Theta* topology we can identify seven different sectors, each one characterized by simpler recursive equations which involve a reduced number of coefficients. The organization into sectors is sketched in Figure 9. For ease of implementation, we decided to write down recursive equations for each sector separately. It should be clear that, despite any optimization in the organization, recursive equations at two loops are more cumbersome than at one loop. All expressions are reported in ancillary files provided along with the present document [10].

We have validated the numerical implementation against analytic results obtained through FeynCalc [100], and in-house codes developed in FORM [107] and in Wolfram Mathematica [108]. The latter consists of a Mathematica notebook that reads the information from the generated skeleton in `HELAC2LOOP` and provides analytic expressions for each amplitude numerator which then is translated in FORTRAN and tested against the numerical results obtained by `HELAC2LOOP`. Extensive validation tests have been performed for amplitude numerators involving gluons and ghosts, to insure that the $d = 4 - 2\epsilon$ terms,

[10] `RECURSIVE_EQUATIONS_ANCILLARY_FILES.tgz`

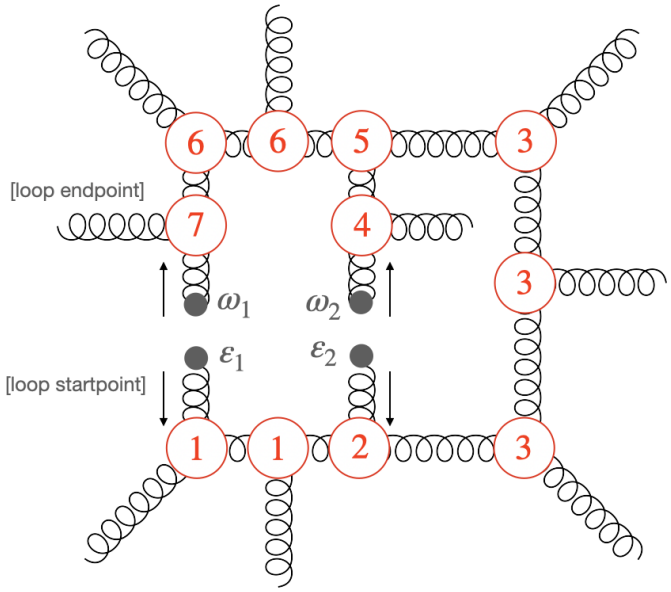

Figure 9: Organization of recursive equations into sectors. Loop vertices labelled with different indices (in red) utilize different set of recursive equations for reconstructing evanescent terms.

involving both the ϵ-components of loop momenta and the explicit ϵ-dependent terms are properly reconstructed. A fully-fledged implementation including all vertices and all possible topologies up to six particles is under development in order to complete numerical reconstruction in $d = 4 - 2\epsilon$ for all scattering amplitudes generated by `HELAC2LOOP`.

5 Summary and Discussion

In this report, we have presented the `HELAC2LOOP` computational framework for the automated numerical evaluation of two-loop scattering amplitudes. `HELAC2LOOP` based on `HELAC` framework [97, 98] constructs all amplitude numerators for a given process. We have analyzed the challenges related to the treatment of color degrees of freedom and in A we list a collection of processes generated by the current version of `HELAC2LOOP` [11]. Following [1] we have implemented the reduction to Master Integrals. For this purpose we have developed `CutTools-2`, that solves cut equations and performs the fitting of the basis coefficients [1]. A novel element in our approach is the introduction of recursive equations that reconstruct numerically the amplitude numerators in $d = 4 - 2\epsilon$ dimensions. We have successfully implemented and tested them at one [12] and two loops. We plan to publish the computer code in the near future. `HELAC2LOOP` is the world's first computational framework for two-loop amplitude evaluation and we expect to have a significant impact in providing the most precise theoretical predictions directly relevant for data analysis at the LHC and the next future high-energy colliders.

[11] The computer code `HELAC2LOOP.tar.xz` is attached to this report.
[12] The computer code `HELAC1LOOP.tgz` is attached to this report.

Acknowledgments

This work is supported by the Hellenic Foundation for Research and Innovation (H.F.R.I.) under the "2nd Call for H.F.R.I. Research Projects to support Faculty Members & Researchers" (Project Number: 02674 HOCTools-II).

A Skeleton Results

Table 1: Summary of the skeleton structures for the QCD corrections to several four-particle SM processes at two loops in full color. The second column specifies the flavors of the particles circulating in the loops. The third column reports the time required to generate the corresponding skeleton. The final column lists the number of individual contributions (numerators) entering the amplitude. All results were obtained using a single CPU core on a personal laptop equipped with an Intel i5 processor and 24GB of RAM.

Process	***Loop-Flavors***	***Time***	***Nums***
$gg \to gg$	$\{g, q, \bar{q}, c, \bar{c}\}$	326 s	74872
$gg \to q\bar{q}$	$\{g, q, \bar{q}, c, \bar{c}\}$	122 s	11336
$gg \to Hg$	$\{g, q, \bar{q}, t, \bar{t}, c, \bar{c}\}$	43 s	3816
$q\bar{q} \to Hg$	$\{g, q, \bar{q}, t, \bar{t}, c, \bar{c}\}$	12 s	392
$gg \to HH$	$\{g, q, \bar{q}, t, \bar{t}, c, \bar{c}\}$	22 s	1424
$q\bar{q} \to HH$	$\{g, q, \bar{q}, t, \bar{t}, c, \bar{c}\}$	4 s	152
$gg \to t\bar{t}$	$\{g, q, \bar{q}, t, \bar{t}, c, \bar{c}\}$	176 s	13120
$q\bar{q} \to t\bar{t}$	$\{g, q, \bar{q}, t, \bar{t}, c, \bar{c}\}$	20 s	1916
$gg \to g\gamma$	$\{g, q, \bar{q}, t, \bar{t}, c, \bar{c}\}$	67 s	7632
$q\bar{q} \to g\gamma$	$\{g, q, \bar{q}, t, \bar{t}, c, \bar{c}\}$	29 s	2932
$gg \to \gamma\gamma$	$\{g, q, \bar{q}, t, \bar{t}, c, \bar{c}\}$	28 s	2848
$q\bar{q} \to \gamma\gamma$	$\{g, q, \bar{q}, t, \bar{t}, c, \bar{c}\}$	8 s	1104
$gg \to H\gamma$	$\{g, q, \bar{q}, t, \bar{t}, c, \bar{c}\}$	30 s	1424
$q\bar{q} \to H\gamma$	$\{g, q, \bar{q}, t, \bar{t}, c, \bar{c}\}$	5 s	176
$gg \to Zg$	$\{g, q, \bar{q}, t, \bar{t}, c, \bar{c}\}$	65 s	7632
$q\bar{q} \to Zg$	$\{g, q, \bar{q}, t, \bar{t}, c, \bar{c}\}$	21 s	2932
$gg \to ZZ$	$\{g, q, \bar{q}, t, \bar{t}, c, \bar{c}\}$	33 s	2848
$q\bar{q} \to ZZ$	$\{g, q, \bar{q}, t, \bar{t}, c, \bar{c}\}$	8 s	1104
$gg \to ZH$	$\{g, q, \bar{q}, t, \bar{t}, c, \bar{c}\}$	24 s	1424
$q\bar{q} \to ZH$	$\{g, q, \bar{q}, t, \bar{t}, c, \bar{c}\}$	5 s	176
$u\bar{d} \to gW^+$	$\{g, u, \bar{u}, d, \bar{d}, t, \bar{t}, c, \bar{c}\}$	19 s	2372
$gg \to W^+W^-$	$\{g, u, \bar{u}, d, \bar{d}, t, \bar{t}, c, \bar{c}\}$	27 s	1424
$u\bar{u} \to W^+W^-$	$\{g, u, \bar{u}, d, \bar{d}, t, \bar{t}, c, \bar{c}\}$	5 s	540
$u\bar{d} \to HW^+$	$\{g, u, \bar{u}, d, \bar{d}, t, \bar{t}, c, \bar{c}\}$	2 s	24
$gg \to Z\gamma$	$\{g, q, \bar{q}, t, \bar{t}, c, \bar{c}\}$	31 s	2848

Continued on next page

Process	*Loop-Flavors*	*Time*	*Nums*
$q\bar{q} \to Z\gamma$	$\{g, q, \bar{q}, t, \bar{t}, c, \bar{c}\}$	8 s	1104
$u\bar{d} \to \gamma W^+$	$\{g, u, \bar{u}, d, \bar{d}, t, \bar{t}, c, \bar{c}\}$	4 s	600
$u\bar{d} \to ZW^+$	$\{g, u, \bar{u}, d, \bar{d}, t, \bar{t}, c, \bar{c}\}$	4 s	600

Table 2: Summary of the skeleton structures for the QCD corrections to some five-particle SM processes at two loops in full color. The structure of the columns is identical to that in table 1, and all results were obtained using the same personal laptop.

Process	*Loop-Flavors*	*Time*	*Nums*
$gg \to ggg$	$\{g, q, \bar{q}, c, \bar{c}\}$	24494 s	1617600
$gg \to q\bar{q}g$	$\{g, q, \bar{q}, c, \bar{c}\}$	9874 s	236360
$gg \to t\bar{t}g$	$\{g, q, \bar{q}, t, \bar{t}, c, \bar{c}\}$	14375 s	270004
$q\bar{q} \to t\bar{t}g$	$\{g, q, \bar{q}, t, \bar{t}, c, \bar{c}\}$	1184 s	36236
$gg \to ggH$	$\{g, q, \bar{q}, t, \bar{t}, c, \bar{c}\}$	2795 s	61192
$q\bar{q} \to ggH$	$\{g, q, \bar{q}, t, \bar{t}, c, \bar{c}\}$	1054 s	6504
$gg \to t\bar{t}H$	$\{g, q, \bar{q}, t, \bar{t}, c, \bar{c}\}$	1748 s	12936
$q\bar{q} \to t\bar{t}H$	$\{g, q, \bar{q}, t, \bar{t}, c, \bar{c}\}$	214 s	5772
$gg \to HHg$	$\{g, q, \bar{q}, t, \bar{t}, c, \bar{c}\}$	1153 s	20680
$q\bar{q} \to HHg$	$\{g, q, \bar{q}, t, \bar{t}, c, \bar{c}\}$	197 s	1996
$gg \to HHH$	$\{g, q, \bar{q}, t, \bar{t}, c, \bar{c}\}$	196 s	8348
$q\bar{q} \to HHH$	$\{g, q, \bar{q}, t, \bar{t}, c, \bar{c}\}$	63 s	748
$gg \to gg\gamma$	$\{g, q, \bar{q}, t, \bar{t}, c, \bar{c}\}$	3741 s	122384
$q\bar{q} \to gg\gamma$	$\{g, q, \bar{q}, t, \bar{t}, c, \bar{c}\}$	1561 s	54252
$gg \to t\bar{t}\gamma$	$\{g, q, \bar{q}, t, \bar{t}, c, \bar{c}\}$	1758 s	54652
$q\bar{q} \to t\bar{t}\gamma$	$\{g, q, \bar{q}, t, \bar{t}, c, \bar{c}\}$	277 s	11464
$gg \to g\gamma\gamma$	$\{g, q, \bar{q}, t, \bar{t}, c, \bar{c}\}$	1653 s	41360
$q\bar{q} \to g\gamma\gamma$	$\{g, q, \bar{q}, t, \bar{t}, c, \bar{c}\}$	416 s	17384
$gg \to \gamma\gamma\gamma$	$\{g, q, \bar{q}, t, \bar{t}, c, \bar{c}\}$	314 s	16032
$q\bar{q} \to \gamma\gamma\gamma$	$\{g, q, \bar{q}, t, \bar{t}, c, \bar{c}\}$	177 s	7064
$gg \to gH\gamma$	$\{g, q, \bar{q}, t, \bar{t}, c, \bar{c}\}$	1233 s	20680
$q\bar{q} \to gH\gamma$	$\{g, q, \bar{q}, t, \bar{t}, c, \bar{c}\}$	266 s	2628
$gg \to H\gamma\gamma$	$\{g, q, \bar{q}, t, \bar{t}, c, \bar{c}\}$	235 s	8016
$q\bar{q} \to H\gamma\gamma$	$\{g, q, \bar{q}, t, \bar{t}, c, \bar{c}\}$	96 s	1176
$gg \to HH\gamma$	$\{g, q, \bar{q}, t, \bar{t}, c, \bar{c}\}$	193 s	8016
$q\bar{q} \to HH\gamma$	$\{g, q, \bar{q}, t, \bar{t}, c, \bar{c}\}$	71 s	896
$gg \to Zgg$	$\{g, q, \bar{q}, t, \bar{t}, c, \bar{c}\}$	4026 s	122384
$q\bar{q} \to Zgg$	$\{g, q, \bar{q}, t, \bar{t}, c, \bar{c}\}$	1830 s	54252
$gg \to t\bar{t}Z$	$\{g, q, \bar{q}, t, \bar{t}, c, \bar{c}\}$	1803 s	54652
$q\bar{q} \to t\bar{t}Z$	$\{g, q, \bar{q}, t, \bar{t}, c, \bar{c}\}$	244 s	11464

Continued on next page

Process	*Loop-Flavors*	*Time*	*Nums*
$gg \to ZZg$	$\{g, q, \bar{q}, t, \bar{t}, c, \bar{c}\}$	1620 s	41360
$q\bar{q} \to ZZg$	$\{g, q, \bar{q}, t, \bar{t}, c, \bar{c}\}$	450 s	17384

Table 3: Summary of the skeleton structures for the QCD corrections to a six-particle and some five-particle SM processes at two loops in full color.

Process	*Loop-Flavors*	*Time*	*Nums*
$gg \to ZZZ$	$\{g, q, \bar{q}, t, \bar{t}, c, \bar{c}\}$	307 s	16032
$q\bar{q} \to ZZZ$	$\{g, q, \bar{q}, t, \bar{t}, c, \bar{c}\}$	146 s	7064
$gg \to ZHg$	$\{g, q, \bar{q}, t, \bar{t}, c, \bar{c}\}$	1240 s	20872
$q\bar{q} \to ZHg$	$\{g, q, \bar{q}, t, \bar{t}, c, \bar{c}\}$	244 s	2652
$gg \to HZZ$	$\{g, q, \bar{q}, t, \bar{t}, c, \bar{c}\}$	201 s	8016
$q\bar{q} \to HZZ$	$\{g, q, \bar{q}, t, \bar{t}, c, \bar{c}\}$	92 s	1176
$gg \to HHZ$	$\{g, q, \bar{q}, t, \bar{t}, c, \bar{c}\}$	186 s	8016
$q\bar{q} \to HHZ$	$\{g, q, \bar{q}, t, \bar{t}, c, \bar{c}\}$	69 s	896
$u\bar{d} \to ggW^+$	$\{g, u, \bar{u}, d, \bar{d}, t, \bar{t}, c, \bar{c}\}$	1592 s	45508
$u\bar{d} \to t\bar{t}W^+$	$\{g, u, \bar{u}, d, \bar{d}, t, \bar{t}, c, \bar{c}\}$	142 s	5692
$gg \to gW^+W^-$	$\{g, u, \bar{u}, d, \bar{d}, t, \bar{t}, c, \bar{c}\}$	1429 s	20680
$u\bar{u} \to gW^+W^-$	$\{g, u, \bar{u}, d, \bar{d}, t, \bar{t}, c, \bar{c}\}$	294 s	5040
$u\bar{d} \to gHW^+$	$\{g, u, \bar{u}, d, \bar{d}, t, \bar{t}, c, \bar{c}\}$	318 s	8468
$u\bar{d} \to HHW^+$	$\{g, u, \bar{u}, d, \bar{d}, t, \bar{t}, c, \bar{c}\}$	37 s	200
$u\bar{u} \to HW^+W^-$	$\{g, u, \bar{u}, d, \bar{d}, t, \bar{t}, c, \bar{c}\}$	41 s	48
$u\bar{d} \to W^+W^-W^+$	$\{g, u, \bar{u}, d, \bar{d}, t, \bar{t}, c, \bar{c}\}$	81 s	2140
$gg \to Zg\gamma$	$\{g, q, \bar{q}, t, \bar{t}, c, \bar{c}\}$	1419 s	41360
$q\bar{q} \to Zg\gamma$	$\{g, q, \bar{q}, t, \bar{t}, c, \bar{c}\}$	390 s	17384
$gg \to ZH\gamma$	$\{g, q, \bar{q}, t, \bar{t}, c, \bar{c}\}$	204 s	8016
$q\bar{q} \to ZH\gamma$	$\{g, q, \bar{q}, t, \bar{t}, c, \bar{c}\}$	89 s	1176
$u\bar{d} \to g\gamma W^+$	$\{g, u, \bar{u}, d, \bar{d}, t, \bar{t}, c, \bar{c}\}$	239 s	9860
$u\bar{d} \to \gamma HW^+$	$\{g, u, \bar{u}, d, \bar{d}, t, \bar{t}, c, \bar{c}\}$	45 s	264
$u\bar{d} \to gZW^+$	$\{g, u, \bar{u}, d, \bar{d}, t, \bar{t}, c, \bar{c}\}$	241 s	9860
$u\bar{d} \to ZHW^+$	$\{g, u, \bar{u}, d, \bar{d}, t, \bar{t}, c, \bar{c}\}$	44 s	264
$gg \to Z\gamma\gamma$	$\{g, q, \bar{q}, t, \bar{t}, c, \bar{c}\}$	288 s	16032
$q\bar{q} \to Z\gamma\gamma$	$\{g, q, \bar{q}, t, \bar{t}, c, \bar{c}\}$	140 s	7064
$gg \to ZZ\gamma$	$\{g, q, \bar{q}, t, \bar{t}, c, \bar{c}\}$	297 s	16032
$q\bar{q} \to ZZ\gamma$	$\{g, q, \bar{q}, t, \bar{t}, c, \bar{c}\}$	146 s	7064
$u\bar{d} \to \gamma\gamma W^+$	$\{g, u, \bar{u}, d, \bar{d}, t, \bar{t}, c, \bar{c}\}$	70 s	3040
$u\bar{d} \to ZZW^+$	$\{g, u, \bar{u}, d, \bar{d}, t, \bar{t}, c, \bar{c}\}$	70 s	3040
$u\bar{d} \to Z\gamma W^+$	$\{g, u, \bar{u}, d, \bar{d}, t, \bar{t}, c, \bar{c}\}$	70 s	3040
$gg \to \gamma W^+W^-$	$\{g, u, \bar{u}, d, \bar{d}, t, \bar{t}, c, \bar{c}\}$	151 s	4054

Continued on next page

Process	*Loop-Flavors*	*Time*	*Nums*
$u\bar{u} \to \gamma W^+W^-$	$\{g, u, \bar{u}, d, \bar{d}, t, \bar{t}, c, \bar{c}\}$	71 s	2410
$gg \to ZW^+W^-$	$\{g, u, \bar{u}, d, \bar{d}, t, \bar{t}, c, \bar{c}\}$	167 s	4054
$u\bar{u} \to ZW^+W^-$	$\{g, u, \bar{u}, d, \bar{d}, t, \bar{t}, c, \bar{c}\}$	70 s	2410
$q\bar{q} \to \gamma\gamma\gamma\gamma$	$\{g, q, \bar{q}, t, \bar{t}, c, \bar{c}\}$	1172 s	40976

Table 4: Summary of the skeleton structures for the QCD corrections to selected SM processes at two loops in the leading-color approximation.

Process	*Loop-Flavors*	*Time*	*Nums*
$q\bar{q} \to ggg$	$\{g, q, \bar{q}, c, \bar{c}\}$	612 s	6348
$gg \to ggg$	$\{g, q, \bar{q}, c, \bar{c}\}$	6730 s	47280
$q\bar{q} \to t\bar{t}H$	$\{g, q, \bar{q}, t, \bar{t}, c, \bar{c}\}$	20 s	276
$gg \to t\bar{t}H$	$\{g, q, \bar{q}, t, \bar{t}, c, \bar{c}\}$	104 s	1198
$q\bar{q} \to \gamma\gamma\gamma\gamma$	$\{g, q, \bar{q}, t, \bar{t}, c, \bar{c}\}$	239 s	3316
$gg \to t\bar{t}q\bar{q}$	$\{g, q, \bar{q}, t, \bar{t}, c, \bar{c}\}$	3546 s	10872
$q\bar{q} \to gggg$	$\{g, q, \bar{q}, c, \bar{c}\}$	34098 s	77616
$gg \to gggg$	$\{g, q, \bar{q}, c, \bar{c}\}$	24783 s	667440

B Vertex functions for pure Yang-Mills QCD

Three-gluon interaction:

$$\begin{aligned} V^{\mu}_{g_1 g_2 \to g}[J^{(n_1)}, J^{(n_2)}] \equiv & \left(J^{(n_2)} \cdot (2\,p^{(n_1)} + p^{(n_2)})\right) J^{(n_1)\,\mu} \\ & - \left(J^{(n_1)} \cdot (p^{(n_1)} + 2\,p^{(n_2)})\right) J^{(n_2)\,\mu} \\ & + \left(J^{(n_1)} \cdot J^{(n_2)}\right) (p^{(n_2)} - p^{(n_1)})^{\mu} \end{aligned} \tag{B.1}$$

Four-gluon interaction:

$$\begin{aligned} V^{\mu}_{g_1 g_2 g_3 \to g}[J^{(n_1)}, J^{(n_2)}, J^{(n_3)}] \equiv & \; 2\left(J^{(n_2)} \cdot J^{(n_3)}\right) J^{(n_1)\,\mu} \\ & - \left(J^{(n_1)} \cdot J^{(n_2)}\right) J^{(n_3)\,\mu} \\ & - \left(J^{(n_1)} \cdot J^{(n_3)}\right) J^{(n_2)\,\mu} \end{aligned} \tag{B.2}$$

Gluon-ghost interactions:

$$V^{\mu}_{\bar{c}_1 c_2 \to g}[J^{(n_1)}, J^{(n_2)}] \;\equiv\; -J^{(n_1)}\, J^{(n_2)}\, p^{(n_1)\mu} \tag{B.3}$$

$$V^{\mu}_{g_1 c_2 \to g}[J^{(n_1)}, J^{(n_2)}] \;\equiv\; \left(J^{(n_1)} \cdot (p^{(n_1)} + p^{(n_2)})\right) J^{(n_2)} \tag{B.4}$$

$$V^{\mu}_{\bar{c}_1 g_2 \to g}[J^{(n_1)}, J^{(n_2)}] \;\equiv\; \left(J^{(n_2)} \cdot p^{(n_1)}\right) J^{(n_1)} \tag{B.5}$$

References

[1] G. Bevilacqua, D. Canko, C. G. Papadopoulos, and A. Spourdalakis, *Towards numerical two-loop integrand reduction*, *JHEP* **11** (2025) 069, [arXiv:2506.07231].

[2] A. Dainese, M. Mangano, A. B. Meyer, A. Nisati, G. Salam, and M. A. Vesterinen, eds., *Report on the Physics at the HL-LHC,and Perspectives for the HE-LHC*, vol. 7/2019 of *CERN Yellow Reports: Monographs*. CERN, Geneva, Switzerland, 2019.

[3] F. Caola, W. Chen, C. Duhr, X. Liu, B. Mistlberger, F. Petriello, G. Vita, and S. Weinzierl, *The Path forward to N^3LO*, in *Snowmass 2021*, 3, 2022. arXiv:2203.06730.

[4] **CMS** Collaboration, *Highlights of the HL-LHC physics projections by ATLAS and CMS*, arXiv:2504.00672.

[5] **FCC** Collaboration, M. Benedikt et al., *Future Circular Collider Feasibility Study Report: Volume 1, Physics, Experiments, Detectors*, arXiv:2505.00272.

[6] A. Huss, J. Huston, S. Jones, M. Pellen, and R. Röntsch, *Les Houches 2023 – Physics at TeV Colliders: Report on the Standard Model Precision Wishlist*, arXiv:2504.06689.

[7] S. Badger, C. Brønnum-Hansen, H. B. Hartanto, and T. Peraro, *First look at two-loop five-gluon scattering in QCD*, *Phys. Rev. Lett.* **120** (2018), no. 9 092001, [arXiv:1712.02229].

[8] S. Badger, C. Brønnum-Hansen, H. B. Hartanto, and T. Peraro, *Analytic helicity amplitudes for two-loop five-gluon scattering: the single-minus case*, *JHEP* **01** (2019) 186, [arXiv:1811.11699].

[9] S. Abreu, F. Febres Cordero, H. Ita, B. Page, and V. Sotnikov, *Planar Two-Loop Five-Parton Amplitudes from Numerical Unitarity*, *JHEP* **11** (2018) 116, [arXiv:1809.09067].

[10] S. Abreu, J. Dormans, F. Febres Cordero, H. Ita, and B. Page, *Analytic Form of Planar Two-Loop Five-Gluon Scattering Amplitudes in QCD*, *Phys. Rev. Lett.* **122** (2019), no. 8 082002, [arXiv:1812.04586].

[11] S. Abreu, J. Dormans, F. Febres Cordero, H. Ita, B. Page, and V. Sotnikov, *Analytic Form of the Planar Two-Loop Five-Parton Scattering Amplitudes in QCD*, *JHEP* **05** (2019) 084, [arXiv:1904.00945].

[12] S. Badger, D. Chicherin, T. Gehrmann, G. Heinrich, J. M. Henn, T. Peraro, P. Wasser, Y. Zhang, and S. Zoia, *Analytic form of the full two-loop five-gluon all-plus helicity amplitude*, *Phys. Rev. Lett.* **123** (2019), no. 7 071601, [arXiv:1905.03733].

[13] H. B. Hartanto, S. Badger, C. Brønnum-Hansen, and T. Peraro, *A numerical evaluation of planar two-loop helicity amplitudes for a W-boson plus four partons*, *JHEP* **09** (2019) 119, [arXiv:1906.11862].

[14] H. A. Chawdhry, M. Czakon, A. Mitov, and R. Poncelet, *Two-loop leading-color helicity amplitudes for three-photon production at the LHC*, *JHEP* **06** (2021) 150, [arXiv:2012.13553].

[15] S. Kallweit, V. Sotnikov, and M. Wiesemann, *Triphoton production at hadron colliders in NNLO QCD*, *Phys. Lett. B* **812** (2021) 136013, [arXiv:2010.04681].

[16] S. Abreu, F. Febres Cordero, H. Ita, B. Page, and V. Sotnikov, *Leading-color two-loop QCD*

corrections for three-jet production at hadron colliders, *JHEP* **07** (2021) 095, [arXiv:2102.13609].

[17] S. Badger, H. B. Hartanto, and S. Zoia, *Two-Loop QCD Corrections to $Wb\bar{b}$ Production at Hadron Colliders*, *Phys. Rev. Lett.* **127** (2021), no. 1 012001, [arXiv:2102.02516].

[18] S. Badger, C. Brønnum-Hansen, D. Chicherin, T. Gehrmann, H. B. Hartanto, J. Henn, M. Marcoli, R. Moodie, T. Peraro, and S. Zoia, *Virtual QCD corrections to gluon-initiated diphoton plus jet production at hadron colliders*, *JHEP* **11** (2021) 083, [arXiv:2106.08664].

[19] S. Badger, H. B. Hartanto, J. Kryś, and S. Zoia, *Two-loop leading-colour QCD helicity amplitudes for Higgs boson production in association with a bottom-quark pair at the LHC*, *JHEP* **11** (2021) 012, [arXiv:2107.14733].

[20] H. A. Chawdhry, M. Czakon, A. Mitov, and R. Poncelet, *Two-loop leading-colour QCD helicity amplitudes for two-photon plus jet production at the LHC*, *JHEP* **07** (2021) 164, [arXiv:2103.04319].

[21] H. A. Chawdhry, M. Czakon, A. Mitov, and R. Poncelet, *NNLO QCD corrections to diphoton production with an additional jet at the LHC*, *JHEP* **09** (2021) 093, [arXiv:2105.06940].

[22] M. Czakon, A. Mitov, and R. Poncelet, *Next-to-Next-to-Leading Order Study of Three-Jet Production at the LHC*, *Phys. Rev. Lett.* **127** (2021), no. 15 152001, [arXiv:2106.05331]. [Erratum: Phys.Rev.Lett. 129, 119901 (2022)].

[23] S. Abreu, F. Febres Cordero, H. Ita, M. Klinkert, B. Page, and V. Sotnikov, *Leading-color two-loop amplitudes for four partons and a W boson in QCD*, *JHEP* **04** (2022) 042, [arXiv:2110.07541].

[24] S. Badger, H. B. Hartanto, J. Kryś, and S. Zoia, *Two-loop leading colour helicity amplitudes for $W\gamma + j$ production at the LHC*, *JHEP* **05** (2022) 035, [arXiv:2201.04075].

[25] S. Badger, M. Czakon, H. B. Hartanto, R. Moodie, T. Peraro, R. Poncelet, and S. Zoia, *Isolated photon production in association with a jet pair through next-to-next-to-leading order in QCD*, *JHEP* **10** (2023) 071, [arXiv:2304.06682].

[26] S. Abreu, G. De Laurentis, H. Ita, M. Klinkert, B. Page, and V. Sotnikov, *Two-loop QCD corrections for three-photon production at hadron colliders*, *SciPost Phys.* **15** (2023), no. 4 157, [arXiv:2305.17056].

[27] B. Agarwal, F. Buccioni, F. Devoto, G. Gambuti, A. von Manteuffel, and L. Tancredi, *Five-parton scattering in QCD at two loops*, *Phys. Rev. D* **109** (2024), no. 9 094025, [arXiv:2311.09870].

[28] G. De Laurentis, H. Ita, M. Klinkert, and V. Sotnikov, *Double-virtual NNLO QCD corrections for five-parton scattering. I. The gluon channel*, *Phys. Rev. D* **109** (2024), no. 9 094023, [arXiv:2311.10086].

[29] G. De Laurentis, H. Ita, and V. Sotnikov, *Double-virtual NNLO QCD corrections for five-parton scattering. II. The quark channels*, *Phys. Rev. D* **109** (2024), no. 9 094024, [arXiv:2311.18752].

[30] S. Badger, H. B. Hartanto, Z. Wu, Y. Zhang, and S. Zoia, *Two-loop amplitudes for $\mathcal{O}\left(\alpha_s^2\right)$ corrections to $W\gamma\gamma$ production at the LHC*, *JHEP* **12** (2025) 221, [arXiv:2409.08146].

[31] S. Badger, H. B. Hartanto, R. Poncelet, Z. Wu, Y. Zhang, and S. Zoia, *Full-colour*

double-virtual amplitudes for associated production of a Higgs boson with a bottom-quark pair at the LHC, *JHEP* **03** (2025) 066, [arXiv:2412.06519].

[32] J. Mazzitelli, V. Sotnikov, and M. Wiesemann, *Next-to-next-to-leading order event generation for Z-boson production in association with a bottom-quark pair*, arXiv:2404.08598.

[33] S. Badger, M. Becchetti, C. Brancaccio, H. B. Hartanto, and S. Zoia, *Numerical evaluation of two-loop QCD helicity amplitudes for $gg \to t\bar{t}g$ at leading colour*, *JHEP* **03** (2025) 070, [arXiv:2412.13876].

[34] B. Agarwal, G. Heinrich, S. P. Jones, M. Kerner, S. Y. Klein, J. Lang, V. Magerya, and A. Olsson, *Two-loop amplitudes for $t\bar{t}H$ production: the quark-initiated N_f-part*, *JHEP* **05** (2024) 013, [arXiv:2402.03301]. [Erratum: JHEP 06, 142 (2024)].

[35] G. De Laurentis, H. Ita, B. Page, and V. Sotnikov, *Compact Two-Loop QCD Corrections for Vjj Production in Proton Collisions*, arXiv:2503.10595.

[36] T. Hahn, *Generating Feynman diagrams and amplitudes with FeynArts 3*, *Comput. Phys. Commun.* **140** (2001) 418–431, [hep-ph/0012260].

[37] P. Nogueira, *Automatic Feynman Graph Generation*, *J. Comput. Phys.* **105** (1993) 279–289.

[38] S. Pozzorini, N. Schär, and M. F. Zoller, *Two-loop tensor integral coefficients in OpenLoops*, *JHEP* **05** (2022) 161, [arXiv:2201.11615].

[39] D. Canko, G. Bevilacqua, and C. Papadopoulos, *Two-Loop Amplitude Reduction with HELAC*, *PoS* **RADCOR2023** (2024) 081, [arXiv:2309.14886].

[40] T. Peraro and L. Tancredi, *Physical projectors for multi-leg helicity amplitudes*, *JHEP* **07** (2019) 114, [arXiv:1906.03298].

[41] T. Peraro and L. Tancredi, *Tensor decomposition for bosonic and fermionic scattering amplitudes*, *Phys. Rev. D* **103** (2021), no. 5 054042, [arXiv:2012.00820].

[42] C. Anastasiou, J. Karlen, and M. Vicini, *Tensor reduction of loop integrals*, *JHEP* **12** (2023) 169, [arXiv:2308.14701].

[43] J. Goode, F. Herzog, A. Kennedy, S. Teale, and J. Vermaseren, *Tensor reduction for Feynman integrals with Lorentz and spinor indices*, *JHEP* **11** (2024) 123, [arXiv:2408.05137].

[44] J. Goode, F. Herzog, and S. Teale, *OPITeR: A program for tensor reduction of multi-loop Feynman integrals*, *Comput. Phys. Commun.* **312** (2025) 109606, [arXiv:2411.02233].

[45] D. A. Kosower and K. J. Larsen, *Maximal Unitarity at Two Loops*, *Phys. Rev. D* **85** (2012) 045017, [arXiv:1108.1180].

[46] P. Mastrolia and G. Ossola, *On the Integrand-Reduction Method for Two-Loop Scattering Amplitudes*, *JHEP* **11** (2011) 014, [arXiv:1107.6041].

[47] Y. Zhang, *Integrand-Level Reduction of Loop Amplitudes by Computational Algebraic Geometry Methods*, *JHEP* **09** (2012) 042, [arXiv:1205.5707].

[48] S. Badger, H. Frellesvig, and Y. Zhang, *Hepta-Cuts of Two-Loop Scattering Amplitudes*, *JHEP* **04** (2012) 055, [arXiv:1202.2019].

[49] P. Mastrolia, E. Mirabella, G. Ossola, and T. Peraro, *Scattering Amplitudes from Multivariate Polynomial Division*, *Phys. Lett. B* **718** (2012) 173–177, [arXiv:1205.7087].

[50] P. Mastrolia, E. Mirabella, G. Ossola, and T. Peraro, *Integrand-Reduction for Two-Loop Scattering Amplitudes through Multivariate Polynomial Division*, *Phys. Rev. D* **87** (2013), no. 8 085026, [arXiv:1209.4319].

[51] R. H. P. Kleiss, I. Malamos, C. G. Papadopoulos, and R. Verheyen, *Counting to One: Reducibility of One- and Two-Loop Amplitudes at the Integrand Level*, *JHEP* **12** (2012) 038, [arXiv:1206.4180].

[52] P. Mastrolia, E. Mirabella, G. Ossola, and T. Peraro, *Multiloop Integrand Reduction for Dimensionally Regulated Amplitudes*, *Phys. Lett. B* **727** (2013) 532–535, [arXiv:1307.5832].

[53] S. Badger, H. Frellesvig, and Y. Zhang, *A Two-Loop Five-Gluon Helicity Amplitude in QCD*, *JHEP* **12** (2013) 045, [arXiv:1310.1051].

[54] H. Ita, *Two-loop Integrand Decomposition into Master Integrals and Surface Terms*, *Phys. Rev. D* **94** (2016), no. 11 116015, [arXiv:1510.05626].

[55] P. Mastrolia, T. Peraro, and A. Primo, *Adaptive Integrand Decomposition in parallel and orthogonal space*, *JHEP* **08** (2016) 164, [arXiv:1605.03157].

[56] T. Peraro, *Analytic multi-loop results using finite fields and dataflow graphs with FiniteFlow*, in *14th International Symposium on Radiative Corrections: Application of Quantum Field Theory to Phenomenology*, 12, 2019. arXiv:1912.03142.

[57] S. Abreu, J. Dormans, F. Febres Cordero, H. Ita, M. Kraus, B. Page, E. Pascual, M. Ruf, and V. Sotnikov, *Caravel: A c++ framework for the computation of multi-loop amplitudes with numerical unitarity*, *Computer Physics Communications* **267** (Oct., 2021) 108069.

[58] F. V. Tkachov, *A Theorem on Analytical Calculability of Four Loop Renormalization Group Functions*, *Phys. Lett.* **100B** (1981) 65–68.

[59] K. G. Chetyrkin and F. V. Tkachov, *Integration by Parts: The Algorithm to Calculate beta Functions in 4 Loops*, *Nucl. Phys. B* **192** (1981) 159–204.

[60] S. Laporta, *High precision calculation of multiloop Feynman integrals by difference equations*, *Int. J. Mod. Phys.* **A15** (2000) 5087–5159, [hep-ph/0102033].

[61] A. von Manteuffel and R. M. Schabinger, *A novel approach to integration by parts reduction*, *Phys. Lett. B* **744** (2015) 101–104, [arXiv:1406.4513].

[62] T. Peraro, *Scattering amplitudes over finite fields and multivariate functional reconstruction*, *JHEP* **12** (2016) 030, [arXiv:1608.01902].

[63] K. J. Larsen and Y. Zhang, *Integration-by-parts reductions from unitarity cuts and algebraic geometry*, *Phys. Rev. D* **93** (2016), no. 4 041701, [arXiv:1511.01071].

[64] Z. Wu, J. Boehm, R. Ma, H. Xu, and Y. Zhang, *NeatIBP 1.0, a package generating small-size integration-by-parts relations for Feynman integrals*, *Comput. Phys. Commun.* **295** (2024) 108999, [arXiv:2305.08783].

[65] X. Liu and Y.-Q. Ma, *Determining arbitrary Feynman integrals by vacuum integrals*, *Phys. Rev. D* **99** (2019), no. 7 071501, [arXiv:1801.10523].

[66] X. Guan, X. Liu, Y.-Q. Ma, and W.-H. Wu, *Blade: A package for block-triangular form improved Feynman integrals decomposition*, *Comput. Phys. Commun.* **310** (2025) 109538, [arXiv:2405.14621].

[67] T. Binoth, J. P. Guillet, and G. Heinrich, *Reduction formalism for dimensionally regulated one loop N point integrals*, *Nucl. Phys. B* **572** (2000) 361–386, [hep-ph/9911342].

[68] G. Heinrich, *Sector Decomposition*, *Int. J. Mod. Phys. A* **23** (2008) 1457–1486, [arXiv:0803.4177].

[69] G. Heinrich, S. P. Jones, M. Kerner, V. Magerya, A. Olsson, and J. Schlenk, *Numerical scattering amplitudes with pySecDec*, *Comput. Phys. Commun.* **295** (2024) 108956, [arXiv:2305.19768].

[70] G. Barucchi and G. Ponzano, *Differential equations for one-loop generalized Feynman integrals*, *J. Math. Phys.* **14** (1973) 396–401.

[71] A. V. Kotikov, *Differential equations method: New technique for massive Feynman diagrams calculation*, *Phys. Lett. B* **254** (1991) 158–164.

[72] A. V. Kotikov, *Differential equations method: The Calculation of vertex type Feynman diagrams*, *Phys. Lett. B* **259** (1991) 314–322.

[73] T. Gehrmann and E. Remiddi, *Differential equations for two loop four point functions*, *Nucl. Phys. B* **580** (2000) 485–518, [hep-ph/9912329].

[74] J. M. Henn, *Multiloop integrals in dimensional regularization made simple*, *Phys. Rev. Lett.* **110** (2013) 251601, [arXiv:1304.1806].

[75] F. Moriello, *Generalised power series expansions for the elliptic planar families of Higgs + jet production at two loops*, *JHEP* **01** (2020) 150, [arXiv:1907.13234].

[76] X. Liu, Y.-Q. Ma, and C.-Y. Wang, *A Systematic and Efficient Method to Compute Multi-loop Master Integrals*, *Phys. Lett. B* **779** (2018) 353–357, [arXiv:1711.09572].

[77] X. Liu and Y.-Q. Ma, *AMFlow: A Mathematica package for Feynman integrals computation via auxiliary mass flow*, *Comput. Phys. Commun.* **283** (2023) 108565, [arXiv:2201.11669].

[78] R.-J. Huang, D.-S. Jian, Y.-Q. Ma, D.-M. Mu, and W.-H. Wu, *Efficient computation of one-loop Feynman integrals and fixed-branch integrals to high orders in ε*, *Phys. Rev. D* **111** (2025), no. 9 094028, [arXiv:2412.21054].

[79] L.-H. Huang, R.-J. Huang, and Y.-Q. Ma, *Tame multi-leg Feynman integrals beyond one loop*, arXiv:2412.21053.

[80] G. Ossola, C. G. Papadopoulos, and R. Pittau, *Reducing full one-loop amplitudes to scalar integrals at the integrand level*, *Nucl. Phys. B* **763** (2007) 147–169, [hep-ph/0609007].

[81] G. Ossola, C. G. Papadopoulos, and R. Pittau, *CutTools: A Program implementing the OPP reduction method to compute one-loop amplitudes*, *JHEP* **03** (2008) 042, [arXiv:0711.3596].

[82] R. K. Ellis, W. T. Giele, and Z. Kunszt, *A Numerical Unitarity Formalism for Evaluating One-Loop Amplitudes*, *JHEP* **03** (2008) 003, [arXiv:0708.2398].

[83] R. K. Ellis, W. T. Giele, Z. Kunszt, and K. Melnikov, *Masses, fermions and generalized D-dimensional unitarity*, *Nucl. Phys. B* **822** (2009) 270–282, [arXiv:0806.3467].

[84] C. F. Berger, Z. Bern, L. J. Dixon, F. Febres Cordero, D. Forde, H. Ita, D. A. Kosower, and D. Maitre, *An Automated Implementation of On-Shell Methods for One-Loop Amplitudes*, *Phys. Rev. D* **78** (2008) 036003, [arXiv:0803.4180].

[85] A. van Hameren, C. G. Papadopoulos, and R. Pittau, *Automated one-loop calculations: A Proof of concept*, *JHEP* **09** (2009) 106, [arXiv:0903.4665].

[86] A. van Hameren, *Multi-gluon one-loop amplitudes using tensor integrals*, *JHEP* **07** (2009) 088, [arXiv:0905.1005].

[87] P. Mastrolia, G. Ossola, T. Reiter, and F. Tramontano, *Scattering AMplitudes from Unitarity-based Reduction Algorithm at the Integrand-level*, *JHEP* **08** (2010) 080, [arXiv:1006.0710].

[88] S. Badger, B. Biedermann, and P. Uwer, *NGluon: A Package to Calculate One-loop Multi-gluon Amplitudes*, *Comput. Phys. Commun.* **182** (2011) 1674–1692, [arXiv:1011.2900].

[89] G. Bevilacqua, M. Czakon, M. V. Garzelli, A. van Hameren, A. Kardos, C. G. Papadopoulos, R. Pittau, and M. Worek, *HELAC-NLO*, *Comput. Phys. Commun.* **184** (2013) 986–997, [arXiv:1110.1499].

[90] T. Peraro, *Ninja: Automated Integrand Reduction via Laurent Expansion for One-Loop Amplitudes*, *Comput. Phys. Commun.* **185** (2014) 2771–2797, [arXiv:1403.1229].

[91] J. Alwall, R. Frederix, S. Frixione, V. Hirschi, F. Maltoni, O. Mattelaer, H. S. Shao, T. Stelzer, P. Torrielli, and M. Zaro, *The automated computation of tree-level and next-to-leading order differential cross sections, and their matching to parton shower simulations*, *JHEP* **07** (2014) 079, [arXiv:1405.0301].

[92] **GoSam** Collaboration, G. Cullen et al., *GOSAM-2.0: a tool for automated one-loop calculations within the Standard Model and beyond*, *Eur. Phys. J. C* **74** (2014), no. 8 3001, [arXiv:1404.7096].

[93] F. Buccioni, J.-N. Lang, J. M. Lindert, P. Maierhöfer, S. Pozzorini, H. Zhang, and M. F. Zoller, *OpenLoops 2*, *Eur. Phys. J. C* **79** (2019), no. 10 866, [arXiv:1907.13071].

[94] M. Becchetti, D. Canko, V. Chestnov, T. Peraro, M. Pozzoli, and S. Zoia, *Two-loop Feynman integrals for leading colour $t\bar{t}W$ production at hadron colliders*, arXiv:2504.13011.

[95] Y. Zhang, *Integrand-level reduction of loop amplitudes by computational algebraic geometry methods*, *Journal of High Energy Physics* **2012** (Sept., 2012).

[96] G. 't Hooft, *A Planar Diagram Theory for Strong Interactions*, *Nucl. Phys. B* **72** (1974) 461.

[97] A. Cafarella, C. G. Papadopoulos, and M. Worek, *Helac-Phegas: A Generator for all parton level processes*, *Comput. Phys. Commun.* **180** (2009) 1941–1955, [arXiv:0710.2427].

[98] A. Kanaki and C. G. Papadopoulos, *HELAC: A Package to compute electroweak helicity amplitudes*, *Comput. Phys. Commun.* **132** (2000) 306–315, [hep-ph/0002082].

[99] G. Bevilacqua, D. D. Canko, A. Kardos, and C. G. Papadopoulos, *Progress on 2—loop Amplitude Reduction*, *J. Phys. Conf. Ser.* **2105** (2021), no. 5 012010.

[100] V. Shtabovenko, R. Mertig, and F. Orellana, *FeynCalc 10: Do multiloop integrals dream of computer codes?*, *Comput. Phys. Commun.* **306** (2025) 109357, [arXiv:2312.14089].

[101] G. Bevilacqua, D. Canko, C. G. Papadopoulos, and A. Spourdalakis, *Two-loop amplitude computation with HELAC*, *PoS* **LL2024** (2024) 051.

[102] D. W. Marquardt, *An algorithm for least-squares estimation of nonlinear parameters*, *Journal of the Society for Industrial and Applied Mathematics* **11** (1963), no. 2 431–441, [https://doi.org/10.1137/0111030].

[103] L. Armijo, *Minimization of functions having lipschitz continuous first partial derivatives*, *Pacific Journal of mathematics* **16** (1966), no. 1 1–3.

[104] E. Anderson, Z. Bai, C. Bischof, S. Blackford, J. Demmel, J. Dongarra, J. Du Croz, A. Greenbaum, S. Hammarling, A. McKenney, and D. Sorensen, *LAPACK Users' Guide*. Society for Industrial and Applied Mathematics, Philadelphia, PA, third ed., 1999.

[105] G. 't Hooft and M. J. G. Veltman, *Regularization and Renormalization of Gauge Fields*, *Nucl. Phys. B* **44** (1972) 189–213.

[106] G. Ossola, C. G. Papadopoulos, and R. Pittau, *On the Rational Terms of the one-loop amplitudes*, *JHEP* **05** (2008) 004, [arXiv:0802.1876].

[107] B. Ruijl, T. Ueda, and J. Vermaseren, *FORM version 4.2*, arXiv:1707.06453.

[108] W. R. Inc., "Mathematica, Version 14.3." Champaign, IL, 2025.